Aus dem Centrum für Muskuloskeletale Chirurgie

der Medizinischen Fakultät Charité-Universitätsmedizin Berlin

DISSERTATION

Traumatic Brain Injury and Bone Healing: Histomorphometric Analyses of Bone Formation in a Wild-type and Leptin-deficiency Murine Model

zur Erlangung des akademischen Grades

Doctor medicinae (Dr. med.)

vorgelegt der Medizinischen Fakultät

Charité – Universitätsmedizin Berlin

Von

Fan Huang

aus Sichuan, VR. China

Datum der Promotion: 18.09.2020

Declaration of contribution to publication

Fan Huang contributed the following to the below listed publication:

R Seemann, F Graef, A Garbe, J Keller, **F Huang**, G Duda, K Schmidt-Bleek, KD Schaser, S Tsitsilonis. Leptin-deficiency eradicates the positive effect of traumatic brain injury on bone healing: histological analyses in a combined trauma mouse model. Journal of musculoskelet & neuronal Interaction, 1;18(1):32-41, 2018.

Contribution: Performing histological staining
Qualitative histomorphometric data collection and evaluation
Mineralized bone area data collection and evaluation

Signature, date and stamp of supervising university professor / lecturer

Signature of doctoral candidate

Contents

Abstract/Zusammenfassung

Abstract

Introduction: It is empirically documented that the combination of traumatic brain injury (TBI) and bone fracture results in an increase of callus formation. However, the underlying mechanisms of this phenomenon have not yet been elucidated. Leptin, which was initially recognized as the regulator of food intake and energy metabolism, has also proven to be important in bone metabolism. In this study, we analyzed fracture healing both with and without concomitant TBI, and qualitative and quantitative histomorphometric analyses were employed on wild-type and leptin-deficiency (ob/ob) mice. We established vivid evidence for the positive effect of TBI on fracture healing as well as the influence of leptin in fracture healing after TBI.

Materials and Methods: 34 female wild-type mice and 31 female ob/ob mice were classified into fracture (wild-type: n = 17, ob/ob: n = 16) and fracture with TBI (wild-type: n = 17, ob/ob: n = 15) subgroups respectively. The fracture was performed as a 0.7 mm gap osteotomy at the left femur followed by external fixation. TBI was induced at the left cortex with a standard controlled cortical impact. The animals were sacrificed at week 3 and week 4 post-operation. For qualitative (bone bridging score) and quantitative histomorphometric analyses (mineralized bone area and density (MdBAr and MdBDn), trabecular microarchitecture), Movat staining was implemented. Tartrate-resistant acid phosphatase (TRAP) staining was performed for osteoblast and osteoclast density analyses.

Results: The group that combined fracture with TBI showed a significant increase of MdBAr and MdBDn, especially in the periosteal area in wild-type mice at week 4 compared with the fracture-only group. However, there were no statistical differences in wild-type mice between the fracture group and fracture with TBI group in

osteoblast and osteoclast density. In terms of fracture healing, ob/ob mice presented compromised bridging score, MdBAr and MdBDn, and osteoblast and osteoclast density compared with the wild-type mice at week 3 and 4. In the ob/ob phenotype, there were no significant differences between the fracture and fracture with TBI groups in bridging score, MdBAr and MdBDn, and osteoblast and osteoclast density in either week 3 or 4.

Conclusion: The positive effect of TBI on fracture healing in wild-type mice was confirmed, while compromised fracture healing in ob/ob mice was also observed. Moreover, TBI did not reverse the negative effect of leptin deficiency on fracture healing. Based on these findings, we suggest leptin to be involved in the acceleration of fracture healing following the signaling cascade of TBI.

Zusammenfassung

Einleitung: In der Klinik sowie in Tiermodellen wurde seit langem eine gesteigerte Kallusbildung und eine damit verbundene verbesserte Knochenheilung nach Schädel-Hirn-Trauma (SHT) beobachtet. Allerdings war der zugrundeliegende Mechanismus des Phänomens bis heute ungeklärt. In diesem Zusammenhang rückt Leptin durch seine nachweisliche wichtige Rolle in der Knochenentwicklung und dem Knochenmetabolismus in den Vordergrund. In dieser Arbeit konnte eine verbesserte Frakturheilung nach SHT durch qualitative und quantitative histomorphometrische Analysen in Wildtyp Mäusen bestätigt werden und der Einfluss von Leptin in der Frakturheilung nach SHT überprüft werden.

Materialien und Methoden: Es wurden 34 weibliche Wildtyp und 31 ob/ob Mäuse in Fraktur (Wildtyp n = 17, ob/ob n = 16) und Fraktur mit SHT (Wildtyp n = 17, ob/ob n = 15) Gruppen eingeteilt. Die Fraktur wurde durch eine 0,7 mm Spalt-Osteotomie im linken Femur und anschließende externe Fixierung durchgeführt. Das SHT wurde durch einen controlled cortical impact (CCT) im linken Cortex induziert. Drei und vier Wochen nach der Operation wurden die Tiere geopfert. Für qualitative (Knochenüberbrückungsscore) und quantitative histomorphometrische Analysen (mineralisierte Knochenfläche und -dichte, trabekuläre Mikroarchitektur) wurde eine Movat-Pentachrom-Färbung durchgeführt. Mittels einer Tartrate-resistant acid phasphatase (TRAP) Färbung wurde die Dichte von Osteoblasten und Osteoklasten bestimmt.

Ergebnisse: Bei den Wildtyp Mäusen mit einer kombinierten Verletzung konnte ein signifikanter Anstieg in der mineralisierten Knochenfläche und -dichte im Vergleich zur Fraktur Gruppe beobachtet werden. Dieser war besonders ausgeprägt in der periostealen Fläche vier Wochen postoperativ. Es wurden keine weiteren statistischen Unterschiede bei den Osteoblasten und Osteoklasten zwischen den untersuchten Gruppen der Wildtyp Mäuse gefunden. Im Frakturmodel wurde gezeigt, dass ob/ob

Mäuse einen verringerten Knochenüberbrückungsscore, mineralisierte Knochenfläche und -dichte, Osteoblasten und Osteklasten Dichte verglichen zu Wildtyp Mäusen drei und vier Wochen postoperativ aufweisen. Innerhalb der Gruppen des ob/ob Phänotyps gab es keine signifikanten Unterschiede zwischen der Fraktur und der Fraktur mit SHT Gruppe in Knochenüberbrückungsscore, mineralisierter Knochenfläche und -dichte sowie in Osteoblasten- und Osteoklastendichte drei und vier Wochen nach Induktion von Fraktur und SHT.

Schlussfolgerung: Der positiv Effekt von SHT auf die Knochenheilung in Wildtyp Mäusen konnte bestätigt werden, sowie die beeinträchtigte Knochenheilung in ob/ob Mäusen. Des Weiteren, konnte ein SHT den Einfluss des fehlenden Leptins in der Knochenheilung nicht umkehren. Basierend auf diesen Ergebnissen vermuten wir eine wichtige Rolle von Leptin bei der SHT vermittelten Steigerung der Knochenheilung.

Abbreviations

ALP	Alkaline phosphatase
BBB	Blood brain barrier
BMC	Bone mineral content
BMD	Bone mineral density
BMP	Bone morphogenetic protein
CCI	Controlled cortical impact
CGRP	Calcitonin gene-related peptide
cm	Centimeter
CNS	Central nervous system
CSF	Cerebrospinal fluid
CXCR-4	CXC motif chemokine receptor 4
EGF	Epidermal growth factor
ELISA	Enzyme-linked immunosorbent assay
g	Gram
GCS	Glasgow Coma Scale
GH	Growth hormone
hFOB	Human fetal osteoblastic cells
HO	Heterotopic ossification
IFMs	Interfragmentary movements
IGF-1	Insulin-like growth factor type 1
kg	Kilogram
MdBAr	Mineralized bone area
MdBDn	Mineralized bone density
mg	Milligram
ml	Milliliter
mm	Millimeter
MSCs	Mesenchymal stem cells
NGF	Nerve growth factor
ob/ob mice	Leptin-deficiency mice
PCR	Polymerase chain reaction
ROI	Region of interest
SD	Sprague-Dawley
SDF-1	Stromal cell-derived factor 1
Tb.Sp	Trabecular separation
Tb.Th	Trabecular thickness
TBI	Traumatic brain injury
TRAP	Tartrate-resistant acid phosphatase
μm	Micrometer

Figure list

Table list

1 Introduction

1.1 The influence of traumatic brain injury (TBI) on fracture healing

Fracture healing is defined as a continuous process of repair of the structure and function of bone tissue [1, Figure 1]. The regeneration process after a fracture can be divided into four consecutive stages: inflammation; soft callus formation; hard callus formation and remodeling. Although each phase can be characterized with distinct features, the entire process is a seamless transition. This repair process is regulated and controlled by a vast number of factors, such as fracture site and type, nutrition, immunity, cells, hormones, cytokines, biomechanical environments and so forth. Chalmers and colleagues [2] considered that three essential conditions are required for the development of uneventful bone healing: osteoprogenitor, osteogenic factor and sustained osteoinductive environment. Over the last few decades, a stream of research has focused on the interaction and signal pathways among these factors; however, the understanding of how TBI affects fracture healing is still awaiting further exploration.

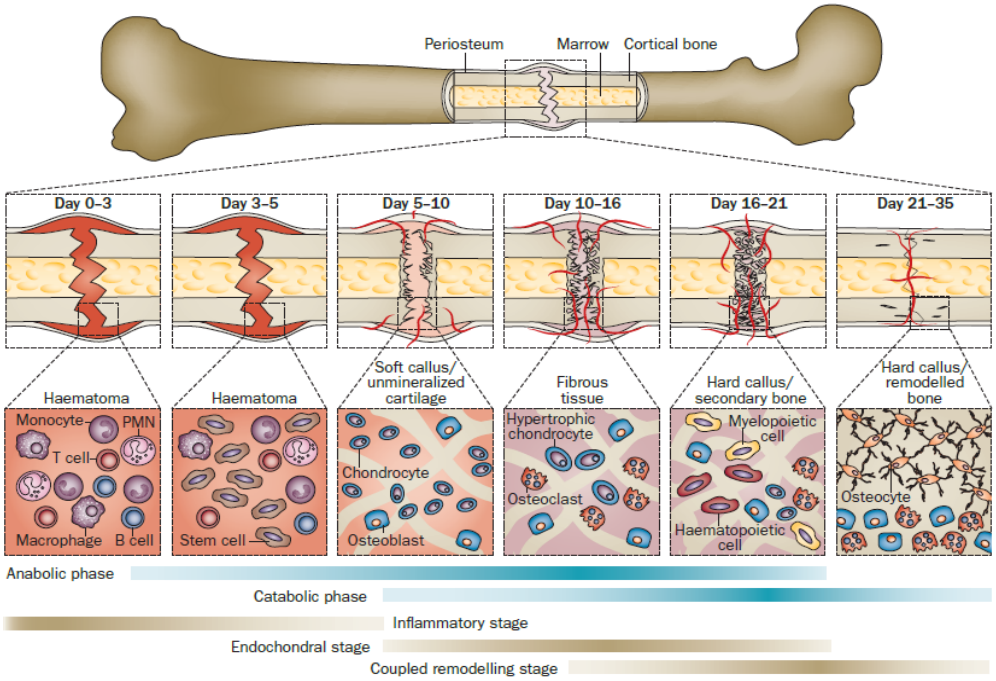

Figure 1: The process of fracture healing. The regeneration of the fracture can be divided into four consecutive stages: inflammation, soft callus formation, hard callus formation and remodeling [1].

TBI is associated with the acceleration of fracture healing and high rates of heterotopic ossification (HO) [3-10]. However, in earlier clinical studies researchers struggled to distinguish between bone callus and HO [3-5, 9, 10]. In 1982, D.E. Garland *et al.* [10] reported that TBI predisposes to callus formation and HO, based on 47 patients who suffered forearm fractures combined with TBI. In 1987, R.F. Spencer *et al*. [9] observed the hypertrophy of bone callus and a high incidence of HO followed by TBI. The authors also documented the histological difference of components between normal callus and callus after TBI.

The studies that followed [11-17] demonstrated the acceleration of bone healing by the radiographic volumetric measurement of callus in patients with TBI, with sample sizes from 28 to 86. In 2012, T.Y. Yang *et al.* [13] performed a clinical trial to evaluate the interaction of TBI on fracture healing in young adults. In this study, 74 closed simple unilateral femoral fracture patients between 16 and 40 years old (mean of age = 24.2) were divided into TBI with fracture group (n = 20), and fracture group (n = 54). Patients with multiple or open fractures, chronic conditions such as diabetes, renal insufficiency or malignancies, and undergoing steroid or immunosuppressive treatments were excluded from the study. All femoral fractures were treated with locked antegrade reamed intramedullary nailing through the standard clinical protocol. The anteroposterior and lateral radiological tests were collected monthly from 1 to 9 months, as well as at month 12. The time of bridging callus and the thickness of callus formation were evaluated by means of conventional radiological images and a modified formula by Spencer *et al.* [9]. The authors found the TBI with fracture group exhibited significantly faster fracture healing (time to bridging) ($p < 0.001$) and higher bone callus thickness ($p < 0.001$) than the fracture group. Moreover, Yang *et al.* demonstrated a tendency of positive correlation between the severity of TBI by Glasgow Coma Scale (GCS) and the speed of fracture healing and final callus thickness formation, although the differences were not statistically significant. D. Cadosch *et al.* [12] found that patients with TBI had a shorter bony bridging formation ($p = 0.01$) and the GSC was positively correlated with the callus formation

($p < 0.05$) and bridging time ($p = 0.04$).

In addition to clinical studies that confirmed the accelerated fracture healing with TBI, animal model experiments found further evidence that TBI leads to enhanced callus formation. In the study by Boes *et al.* [18], 43 7-9 month-old adult Sprague-Dawley (SD) rats were grouped into isolated femoral fracture ($n = 20$) and fracture combined with TBI ($n = 23$) serving as variable. Fracture healing was assessed by bone callus diameter and biomechanical testing 3 weeks postoperatively. The combined group was found to have a reduced callus diameter, but increased stiffness compared with the fracture group. Additionally, Song *et al.* [19] investigated the bone mineral density (BMD) and bone mineral content (BMC) of the newly-formed callus between TBI-fracture group and fracture-only group by micro-CT in SD rats. In the 4th week, the TBI-fracture group showed significantly higher BMD ($p < 0.05$) and BMC ($p < 0.01$) than those in the fracture-only group. Interestingly, Wang *et al.* [20] and Zhang *et al.* [21] found TBI and spinal cord injury could both accelerate fracture healing in a SD rat model, respectively.

The pathophysiological mechanisms of accelerated fracture healing after TBI remain unknown. The cerebral inflammation cascade after trauma has been studied comprehensively. The study by Gautschi *et al.* [22] suggested that cerebrospinal fluid (CSF) could be a possible source of systemic osteogenic factors after TBI. Blood plays an important role as a biologic link between traumatized brain tissue and peripheral ossification. The blood brain barrier (BBB) is a complex system that prevents the exchanges of substances between CSF and blood, and is composed of the neurovascular unit, a combination of brain microvascular endothelial cells, astrocytes, pericytes, perivascular macrophages and basal lamina [23]. A number of studies have reported that the complement, chemokines and cytokines, might play important parts in connecting the TBI and fracture healing by diffusing through BBB damage [18, 24-27].

Cadosch and Gautschi *et al.* [12, 22, 28] showed the osteoinductive effects of the

serum (6, 24, 72, 168 hours post-injury) and CSF (12 hours post-injury) from patients with TBI. In their studies, the serum and CSF from patients with combined TBI and femoral fracture significantly accelerated the proliferation rates of human fetal osteoblastic cells (hFOB) and primary osteoblast. Boes *et al.* [18] showed that the sera of rats with TBI and fracture exhibited significantly higher osteoinductive potential to proliferate mesenchymal stem cells (MSCs) *in vitro* compared to those from rats with isolated fracture. Results from Yang *et al.* [29] showed that the serum from TBI Wismar rats promoted *in vitro* proliferation of osteoblastic MC3T3-E1 cells.

Apart from the osteoinductive effects of serum and CSF observed in TBI, some studies further identified osteoinductive factors after TBI. On the one hand, Yan *et al.* [30] revealed that the expression of bone morphogenetic protein (BMP)-10 within 3 mm depth at the impaired cerebral cortex of mice was strongly induced, compared with that in the control group at day 3 postoperatively. On the other hand, Gautschi *et al.* [22] investigated osteoinductive factors in the CSF of clinical TBI patients, and the results indicated that BMP-2, -4, or -7, which were measured by enzyme-linked immunosorbent assay (ELISA), were unlikely to be the putative osteoinductive factors. Also, Gautschi *et al.* [11] revealed that alkaline phosphatase (ALP), runt-related transcription factor 2 (Runx2), cathepsin K and serine protease 7 were augmented in serum of TBI with fracture patients, compared to fracture-only and control groups. Liu *et al.* [31] showed significantly increased mRNA expression of SDF-1 (stromal cell-derived factor 1) and its receptor CXCR-4 (CXC motif chemokine receptor 4) in newly-formed bone callus in TBI with fracture mice, compared to fracture only mice. Song *et al.* [19] collected serum, brain and muscles surrounding the fracture sites at 24, 48, 72 and 168 hours after injury, and revealed a high concentration of calcitonin gene-related peptide (CGRP) in the TBI-fracture group. Yang *et al.* [29] observed the enhanced expression of osteocalcin in serum from TBI rats, and furthermore, they found that the proliferation of the mouse osteoblastic cell line MC3T3-E1 was positively regulated in the presence of arachidonic acid, which could be important in accelerating the procedure of fracture

healing after TBI. Osteogenetic hormone factors in serum, such as growth hormone (GH), insulin-like growth factor type 1(IGF-1), epidermal growth factor (EGF) and nerve growth factor (NGF) levels, significantly increased during fracture healing in patients with TBI, which may be implicated in the procedure of fracture healing [32,33].

However, the mechanism and the signal pathway of these factors to accelerate fracture healing and to increase bone callus formation after TBI has yet to be elucidated. In recent years, scholars have discovered that the central nervous system (CNS) plays a key role in the regulation of metabolism and the repair of bone by a systemic cascade of factors. Among these factors, leptin was proved to be an integral part of bone development and healing. Yan *et al.* [34] demonstrated the co-elevated concentration of leptin with GH and IGF-I in the serum and CSF of a rabbit TBI model. Furthermore, the injection of leptin in the cerebellomedullary cistern promoted fracture healing in TBI, compared to their control group without this injection.

1.2 Leptin and the leptin-deficient mouse model

Leptin, the product encoded by the "obese" gene, is a cytokine-like proteic hormone of 16 kDa mainly synthesized and secreted by adipocytes in white adipose tissue [35]. It has been shown that leptin is a regulator of food intake and energy metabolism, and is additionally involved in angiogenesis and homeostasis, while affecting the reproductive, cardiovascular and immune systems, as well as brain development through the central and peripheral nervous system [36-42].

The leptin-deficiency (ob/ob) mice were first reported in 1950 as a natural spontaneous mutation, and appeared with obesity and type II diabetes [43]. In 1994, Zhang *et al.* [35] identified the phenotype ascribed to obese gene mutation. Ob/ob mice are homozygous of the recessive mutation of the obese gene at chromosome 6. Therefore, due to the hunger-suppressing effect of leptin, ob/ob mice show four-times

heavier body weight than wild-type mice. Consequently, compensatory hyperglycemia and hyperinsulinemia are observed [44, 45].

In addition to its effects on energy metabolism, leptin also has an impact on bone development and metabolism. In 2000, Ducy and colleagues [46] demonstrated that ob/ob mice had a higher bone volume of vertebrae and femur than wild-type mice in radiographic and histological analyses and biomechanical testing, while the intracerebroventricular infusion of leptin resulted in bone loss in both ob/ob and wild-type mice. In 2002, Takeda and Ducy's group [47] extended their research and elucidated the antiosteogenic function of leptin that regulates bone formation by the hypothalamus-β-adrenergic receptor axis via the sympathetic nervous system.

However, some studies reported different patterns of bone mass in ob/ob mice compared with wild-type mice. Hamrick *et al.* [48] suggested that the response of bone to altered leptin signaling was not uniform throughout femur and vertebrae. They found that ob/ob mice presented significantly shorter femora, with lower BMC and BMD, cortical thickness, and trabecular bone volume, in contrast to their strikingly increased vertebral length, lumbar BMC and BMD, and trabecular bone volume compared to wild-type mice. Ivaniec *et al.* [49] and Turner *et al.* [50] confirmed the findings of Hamrick by micro-CT. Moreover, the selective central recombinant adeno-associated virus-leptin administration by intracerebroventricular injection reversed the skeletal abnormalities. Steppan *et al.* [51] and Turner *et al.* [50] reported that peripheral injections of leptin augmented total BMC and BMD, femoral length, and trabecular and cortical mineral content in ob/ob mice compared with the sham group, and even with the wild-type group[50].

However, in a recent paper by Yue *et al.* [52], the Prx1-Cre; $Lepr^{fl/fl}$ mouse was explored as a model of the direct peripheral influence of leptin between osteogenesis and adipogenesis. In this mouse, a conditional deleted leptin receptor from MSCs of extremities is observed, but not from the axial skeleton or CNS, thus leading to normal body weight and glycemia. They found that the Prx1-Cre; $Lepr^{fl/fl}$ mice

showed higher bone volume, number, thickness, and BMD of trabeculae in the femoral metaphysis. In *in vivo* experiments, the Prx1-Cre; $Lepr^{fl/fl}$ mice exhibited higher bone volume, trabecular number and thickness in fracture callus, which indicated that the leptin receptor negatively regulated fracture healing. They further suggested that the peripheral leptin receptor signaling promoted adipogenesis and inhibited osteogenesis by MSCs, but that deletion of leptin receptor in osteoblasts could not affect osteogenesis or adipogenesis. On the other hand, Gordeladze *et al.* [53] found on the other side that leptin was protective against apoptosis of osteoblasts, and induced the differentiation of osteoblasts into osteocytes. Thomas *et al.* [54] suggested that leptin promotes the differentiation of MSCs into osteoblasts and their inhibition into adipocytes. Based on the above-mentioned previous studies, a dual signal pathway mechanism of leptin could be speculated.

1.3 The effect of Leptin on TBI and fracture healing

Wang *et al.* [55] reported that the concentration of leptin in serum in rats with a combined injury (TBI and fracture) group was significantly higher than that in the groups with isolated injury (TBI or fracture respectively) at week 4 and week 8. The percentage of leptin positive cells in the callus of the groups with the combined injury was significantly higher than that of the fracture group. Furthermore, Wei *et al.* [56] showed that serum leptin significantly increased in the fracture, TBI and TBI with fracture groups compared with the control group at week 2 after trauma. Yan *et al.* [34] found that leptin in CSF and leptin in serum presented a positive correlation at 24 hours after TBI, while the concentration of fluorescein isothiocyanate-label leptin in the brain after TBI was higher than in sham-operated animals. However, polymerase chain reaction (PCR) evidence did not support the existence of differences in expression of leptin in brain between the TBI and control group. In clinical practice, Lin *et al.* [57] found that serum leptin level in the TBI with fracture patients was substantially higher than that of the control group.

To summarize, while a large number of factors have been explored in the accelerated fracture healing caused by TBI, the interaction of TBI and fracture healing, as well as the mechanism of how leptin affected the above-mentioned factors to regulate fracture healing are still open for dedicated research.

1.4 Aim of the present study

As mentioned earlier, leptin could prove an important factor in accelerated fracture healing with TBI via the central hypothalamic and direct peripheral signal pathways. The purpose of the present study is to further evaluate the effects of TBI on fracture healing, by observing and analyzing the fracture healing procedure with and without TBI at the absence of leptin in ob/ob mice by histomorphometry.

2 Materials and Methods

2.1 Experimental design

All experiments were performed according to the policies and principles set forth by the German Animal Welfare Act (Federal Law Gazette I, p.1094) and the National Institutes of Health Guide for Care and Use of Laboratory Animals, and at the same time approved by the State Office for Health and Social Affairs of Berlin (Landesamt für Gesundheit und Soziales, Berlin, G 0009/12).

The animals were assigned to two groups (wild-type group and ob/ob group). Female C57/Black6N mice were chosen as wild-type models (Charles River, Sulzfeld, Germany, age: 12-15 weeks, body weight: 22±3 g), while female B6.V-Lep^{ob}/JRj mice, which were the obese mice derived from C57BL/6J mice, were selected as the ob/ob models (Janvier, Saint Berthevin, France, age: 10-12 weeks, body weight: 50±5 g). Each animal phenotype was subcategorized into fracture and fracture with TBI subgroups. The animals were sacrificed at week 3 and week 4 post operation (Figure 2).

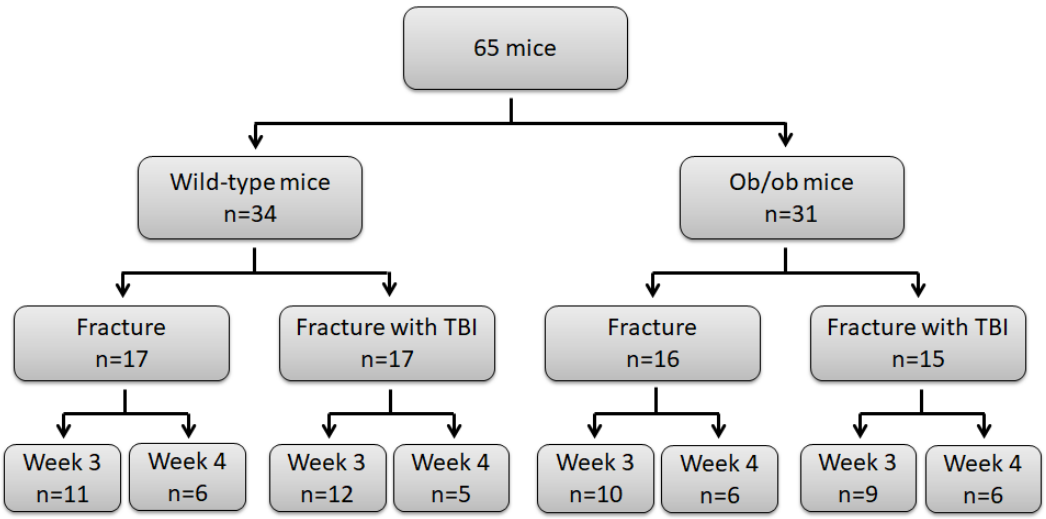

Figure 2: Overview of division of experimental mice. 34 wild-type mice and 31 ob/ob mice were divided into fracture and fracture with TBI subgroups. The mice were sacrificed at week 3 and week 4 postoperatively.

2.2 Accommodation and nutrition of the animals

All mice were housed in the animal experimental facility of the Campus Virchow-Klinikum of the Charité – Univerisitätsmedizin Berlin (animal husbandry ISO 9000/2008) under conditions of controlled temperature (20 ± 2 ℃) and humidity (55%) in a standard 820 cm^2 Type III cage (Euronorm). Wood chips and cellulose cloths were used as backgrounds. The mice were provided with pelleted concentrated feed (Ssniff, Soest, Germany) and tap water via the grid of the cage lid *ad libitum*. A 12 hour light-darkness cycle was controlled by timer. Daytime (light) was from 06:00 to 18:00 and the night-time (dark) was from 18:00 to 06:00.

2.3 Surgical procedure

2.3.1 Preoperative management and anesthesia

The trauma model adopted in this study was the combined trauma model of fracture and TBI as per Tsitsilonis *et al.* [58]. All surgical procedures were performed on a heating pad (37 ℃, Beurer, Ulm, Germany). Anesthetic induction was performed in a semi-open pot with continuous inhaled gas, with 2% isoflurane (FORENE, Abbott, Wiesbaden, Germany) in combination with 0.3% O_2 and 0.5% N_2O (0.5 and 0.3 liter/minute). Next, 0.02 ml antibiotic clindamycin and analgesic buprenorphine (0.1 ml/kg, TEMGESIC, Reckitt Benckiser, Mannheim, Germany) were administrated subcutaneously. Eye ointment (Bepanthen ophthalmic and nasal ointment, Bayer, Leverkusen, Germany) was applied to eyeballs to avoid eye drying. Head immobilization was performed by a stereotactic system (Stoelting, Wood Dale, Illinois, USA) with two lateral studs fixed in the external auditory meatus. The maintenance of anesthesia was performed using a semi-open inhaled system with 1.6% isoflurane (FORENE, Abbott, Wiesbaden, Germany), 0.3% O_2 and 0.5% N_2O (0.5 and 0.3 liter/minute).

2.3.2 Bone fracture model

The bone fracture model was performed with the standardized femoral osteotomy with an external fixator [59]. The external fixator (MouseExFix, Research Implant System, Davos, Switzerland) [60] consists of a rigid polymer block (length 10.4 mm) with four holes for proximal and distal fixation, and four corresponding metal pins (diameter 0.45 mm). Skin preparation was conducted, with hair being trimmed with dissecting scissors and depilatory in the anterolateral region of the thigh. 10% Braunol (B. Braun Melsungen AG, Melsungen, Germany) was applied for skin disinfection. For mid-diaphyseal access to the femur, a 2 cm lateral longitudinal incision was created from the hip joint to knee joint. The femur was exposed by transection of the fascia lata, then blunt separation of vastus lateralis and biceps femoris. The sciatic nerve was protected carefully. Subsequently, soft tissues surrounding the diaphysis where the osteotomy was to be operated were blunt loosened (Figure 3a). The first borehole was drilled with a fine drill (diameter 0.45 mm) at the condyle of the distal femoral metaphysis, vertically to the femoral axis and cortical surface. The first pin with the polymer block was then screwed and fixed, and the position of the fixator was determined (Figure 3b), followed by the remaining drillings for pins through the polymer block of the external fixator (Figure 3c). After rigid external fixation, a 0.70 mm osteotomy was performed at the midpoint between the interior pins with a Gigli wire saw (RISystem, Davos, Switzerland) (Figure 3d and 3e). Incision closure was achieved by donati suture with Ethilon 5-0 suture (Ethicon, Johnson & Johnson, Norderstedt, Germany) (Figure 3f).

(a) Femoral diaphysis exposure

(b) Fixation of first pin with the block

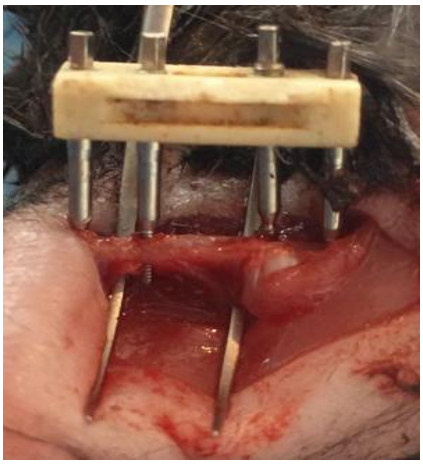

(c) Settlement of external fixator

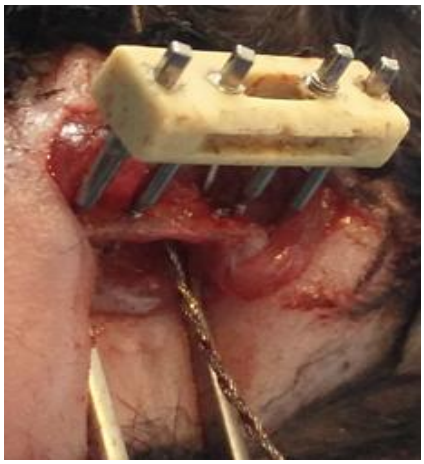

(d) Osteotomy by wire saw

(e) 0.7 mm osteotomy gap

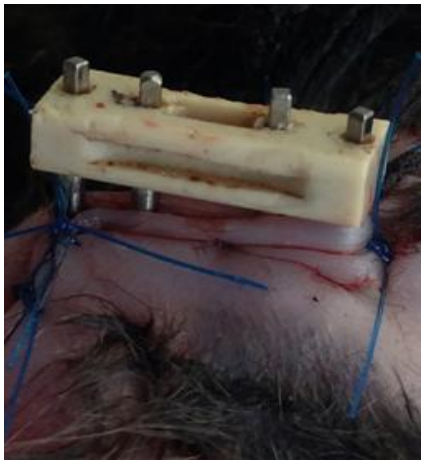

(f) Closure and suture of incision

Figure 3: Femoral fracture procedure: (a) exposure of femoral diaphysis. (b) first pin with block was screwed and fixed. (c) external fixator was settled with four pins. (d) osteotomy was performed by wire saw. (e) 0.7 mm osteotomy gap. (f) closure and suture of incision with Ethilon Suture 5-0.

2.3.3 Traumatic brain injury (TBI) model

The TBI model was performed with the standardized technique of controlled cortical impact (CCI) (Figure 4a) [61-63]. The head of the animal was stereotactically fixed by external auditory meatus (Stoelting, Wood Dale, Illinois/USA). Skin preparation was done with hair being trimmed with dissecting scissor and depilatory in the parietotemporal region of the head. 10% Braunol (B. Braun Melsungen AG, Melsungen, Germany) was applied for skin disinfection. In addition to inhaled systemic analgesia, 0.5% bupivacaine (1 ml/kg, bupivacaine-RPR-Actavis, Actavis GmbH & Co. KG, Munich, Germany) was administrated into the region of operation subcutaneously. Cross incision was created with a 1.5 cm incision along the sagittal suture, then extended perpendicularly along the lambdoidal suture to the distal of the temporal bone (Figure 4b). Under the microscope (OPMI-6 SFC surgical microscope, Carl Zeiss AG, Oberkochen, Germany), the temporalis muscle was partially detached from the cranial bone by bipolar coagulation (Erbotom Bipolar, Erbe Elektromedizin, Rangendingen, Germany). The 7×7 mm craniotomy was performed by electric ball mill (diameter 1.2 mm) (Minimot 40, Proxxon, Föhren, Germany) (Figure 4c). Meanwhile, the dura mater was maintained carefully (Figure 4d).

The animal was subsequently transferred to the automatic pneumatic cortical impact device (AmScien Instruments, Richmond, Virginia, USA). The TBI model was performed with defined parameters (firing pin: diameter 5.0 mm, impact angle: 45 °, penetration depth: 0.25 mm, impact speed: 3.5 m/s and contact duration: 150 ms). The firing pin was adjusted to collimate to the dura mater of the bone window (Figure 4e). Finally, the previously preserved cranial bone was repositioned with dental cement (Hoffmann, Berlin, Germany) (Figure 4f). Incision closure was performed with Ethilon 5-0 suture (Ethicon, Johnson & Johnson, Norderstedt, Germany). All TBI operations were followed by femoral fracture operations sequentially.

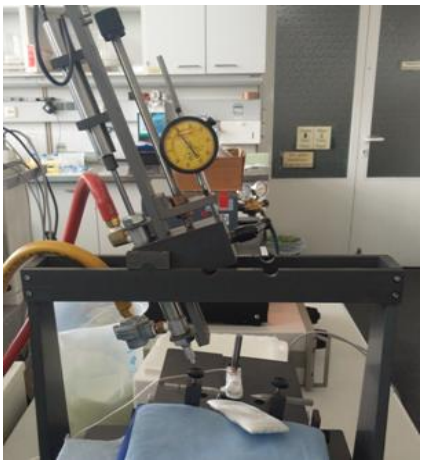

(a) Controlled cortical impact device

(b) Exposure of crania

(c) Craniotomy by electric ball mill

(d) Bone window and dura mater

(e) Dura mater after TBI

(f) Reposition of crania with dental cement

Figure 4: Traumatic brain injury (TBI) procedure: (a) TBI was performed with a standard controlled cortical impact device. (b) exposure of crania by cross incision. (c) the 7×7 mm bone window was created with electric ball mill. (d) bone window and intact dura mater. (e) hyperaemia of dura mater after TBI. (f) the crania was repositioned and adhered with dental cement.

2.3.4 Postoperative management and organ harvesting

Animals were kept in a thermostat-regulated cage with a light lamp for 2 hours for anesthetic resuscitation. Analgesic therapy was administrated with tramadol (Tramal, 100mg/ml, Grünenthal, Aachen, Germany) in the drinking water (8 drops/250 ml) for 3 days postoperatively. In case of external injury (bite) and incisional healing disorders, tetracycline spray (oxytetracycline hydrochloride, Norbrook Laboratories Ltd, Northamptonshire, England) was applied.

The animals were sacrificed by cervical dislocation at week 3 and week 4 postoperatively. Intraperitoneal injections of medetomidine (0.3 mg/kg, Domitor, Orion Pharma, Bad Homburg, Germany) and ketamine (60 mg/kg, Ketamin, Actavis, Munich, Germany) were performed before each sacrifice. To avoid damage to the callus, the femora were harvested with the external fixator and slight soft tissue surrounding the fracture gap.

2.4 Histology and histomorphometry

2.4.1 Preparation of cryosection

The harvested femora were kept in 4% paraformaldehyde for 24 hours at 4 ℃, and subsequently incubated in escalating concentrations of glucose solution (10%, 20% and 30% respectively) for 24 hours. The femora were embedded in the molds with embedding medium (SCEM Embedding Medium, Section Lab Co Ltd., Hiroshima, Japan). The femora were adjusted to a standardized position in the molds for cutting. The embedding molds were immersed into a beaker with hexane [C_6H_{14}] (n-Hexan > 95, Carl Roth GmbH & Co. KG, Karlsruhe, Germany), and the beaker was cooled down in acetone (Acetone 3221, SIGMA ALDRICH, Steinheim, Germany) and dry ice bath in the cooling tank. When the embedding medium hardened, the external fixators were removed, and the blocks were stored at -80 ℃. Serial sections of 7 µm were cut by cryostat microtome (Leica CM3050S, Leica Microsystems, Nussloch,

Germany), and subsequently transferred onto microscope slides by cryofilm (Cryofilm type II C, Section Lab Co Ltd., Hiroshima, Japan). The sections were dried at room temperature for 30 minutes, and were then frozen in the preparation box at -80 ℃.

2.4.2 Movat pentachrome staining

In 1955, Movat [64] reported a novel staining method showing collagen fibers, proteoglycans, muscle fibers, elastic fibers and fibrin with five different colors. Olah *et al.* [65] applied Movat pentachrome staining for undecalcified bone tissues, and successfully distinguished between bone, cartilage, muscle and other connective tissue. Moreover, Movat pentachrome staining was able to identify the calcified and non-calcified situation of bone and cartilage effectively (Figure 5).

Staining Protocol

1. Air drying ..... 30 minutes

2. Aqua destillat ..... 5 minutes

3. 3% Acetic acid ..... 3 minutes

4. 1% Alcian blue in 3% Acetic acid, pH 2.5 ..... 30 minutes

5. 3% Acetic acid ..... short rinse

6. Aqua destillata ..... 5 minutes

7. Alkaline alcohol (10 ml NH_4OH + 90 ml 96% alcohol) ..... 1 hour

8. Tap water, flowing ..... 10 minutes

9. Aqua destillata ..... short immerse

10. Weigert's iron hematoxylin ..... 10 minutes

11. Tap water, flowing ..... 15 minutes

12. Brilliant crocein/acid fuchsin ..... 15 minutes

13. 0.5% acetic acid ..... short rinse

14. 5% phosphotungstic acid ..... 20 minutes

15. 0.5% acetic acid ..... 2 minutes

16. 100% alcohol ..... 3×5 minutes

17. Safran du Gatinais ..... 1 hour

18. 100% alcohol, wash ..... 3 times

19. 100% alcohol ..... 2 minutes

20. Xylol ..... 2×5 minutes

21. Coverslip

Coloring results

Mineralized bone: ..... bright yellow

Mineralized cartilage: ..... blue-green

Cartilage tissue: ……..... green to yellow

Osteoid: ..... dark red

Muscle: ..... red

Elastic fibers: ..... red

Nuclei: ..... blue-black

Cytoplasm: ..... reddish

Acidic glycosaminoglycans: ..... bright light blue

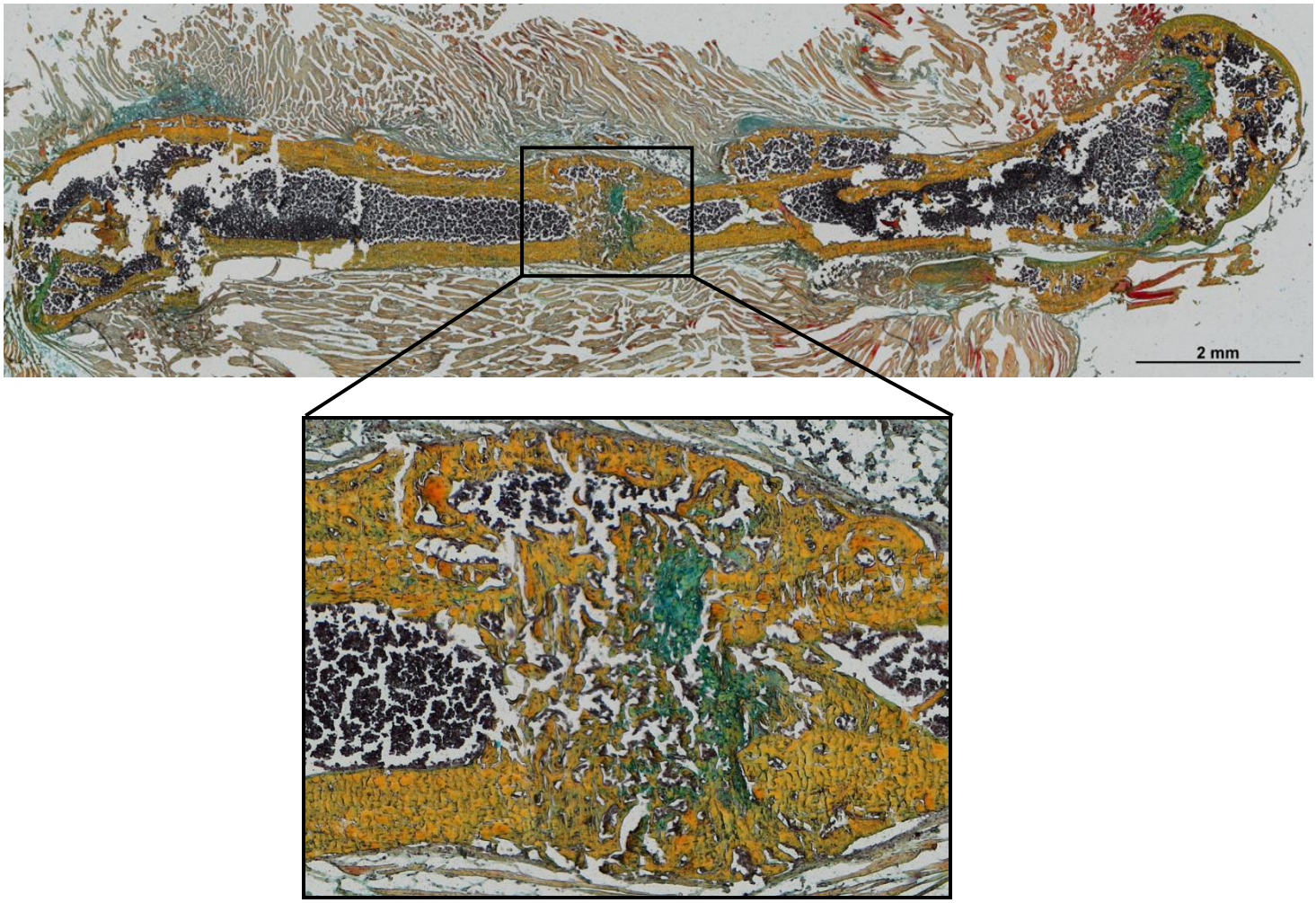

Figure 5: Movat pentachrome staining of the femur. Mineralized bone is yellow. Cartilage is green. Connective tissue is grey. Muscle is in red. The ROI of the fracture gap is zoomed in.

2.4.3 Tartrate-resistant acid phosphatase (TRAP) staining

Tartrate-resistant acid phosphatase (TRAP), the fifth type of acid phosphatase isozyme (0-5), is a glycosylated monomeric metalloprotein enzyme expressed in mammals, and mainly specifically distributed in the cytoplasm of mature osteoclasts. TRAP was considered as an important marker enzyme to identify osteoclasts. TRAP staining makes use of the azo coupling mechanism to dye zymophores with Parafuchsin to reddish brown [66] (Figure 6).

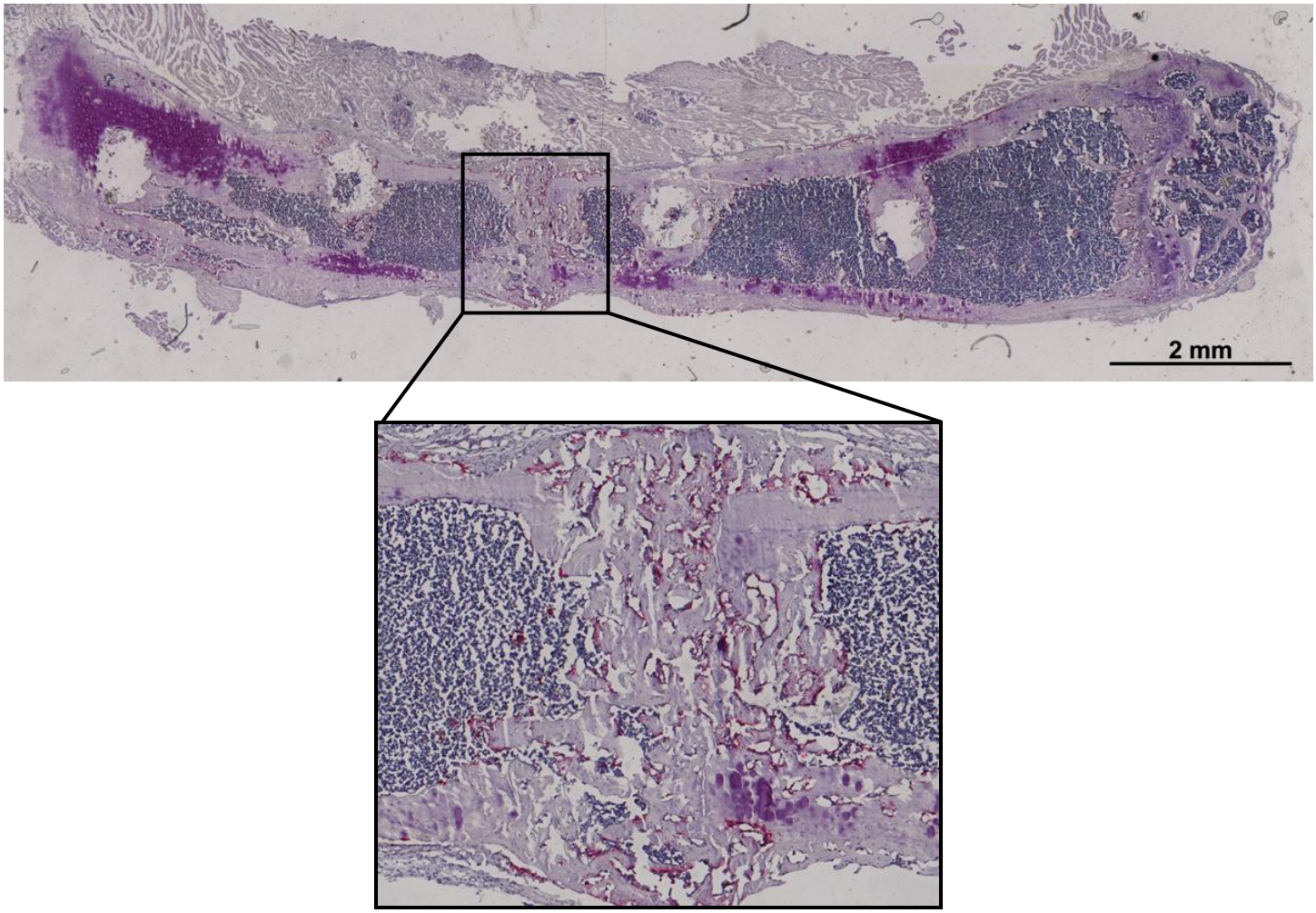

Figure 6: TRAP staining of the femur. Mineralized bone is purple. Cytoplasm of the osteoclasts is reddish-brown. Cytoplasm of the osteoblasts is grey. The nucleus is blue. The ROI of the fracture gap is zoomed in.

Staining Protocol

1. Aqua destillata..... 2 minutes

2. TRAP buffer ..... 10 minutes

3. TRAP solution, 37 °C, microscope control…..... 2-4 hours

4. Aqua destillata..... short rinse

5. Counterstain, Mayer's hematoxylin ..... 3 minutes

6. Tap water ..... 10 minutes

7. Coverslip in aquatex

Coloring results

Mineralized bone..... purple

Cytoplasm of osteoclast ..... reddish-brown

Cytoplasm of osteoblast .....grey

Nucleus ..... blue

2.4.4 Qualitative and quantitative histomorphometric analyses

Before qualitative and quantitative histomorphometric analyses, digital mosaic photographs were obtained by microscope (Zeiss Axioskop 40, Carl Zeiss MicroImaging, Göttingen, Germany) and reassembled by removing the overlaps with AxioVision (Carl Zeiss MicroImaging, Göttingen, Germany).

ImageJ (National Institutes of Health, USA) was used to calculate the bone fracture healing, with the qualitative ABCD bridging score following Mehta *et al.* [67], and using the quantitative histomorphometric analysis of Movat pentachrome staining. In the ABCD bridging score evaluation, A was defined as complete bone bridging with four cortices bridged by callus, B was described as partial bone bridging with two or three cortices bridged by callus, C showed callus formation without cortex bridging and D was classified as pseudarthrosis with little callus formation in the fracture gap. Two experienced reviewers observed independently, and a third reviewer was involved when a discrepancy occurred (Figure 7).

Quantitative histomorphometric analysis concentrated on the area of different tissue of the fracture gap, within a determined 1 mm wide of region of interest (ROI) (Figure 8). The following parameters were included: total area, cortex area, total mineralized bone area (MdBAr), total mineralized bone density (MdBDn, calculated by MdBAr/total tissue area), endosteal MdBDn, periosteal MdBDn, cartilage area, and connective tissue area. In addition, the trabecular bone score which depicted the micro

architecture of cancellous bone of callus was obtained, such as trabecular thickness (Tb.Th) and trabecular separation (Tb.Sp) [68] (Figure 9).

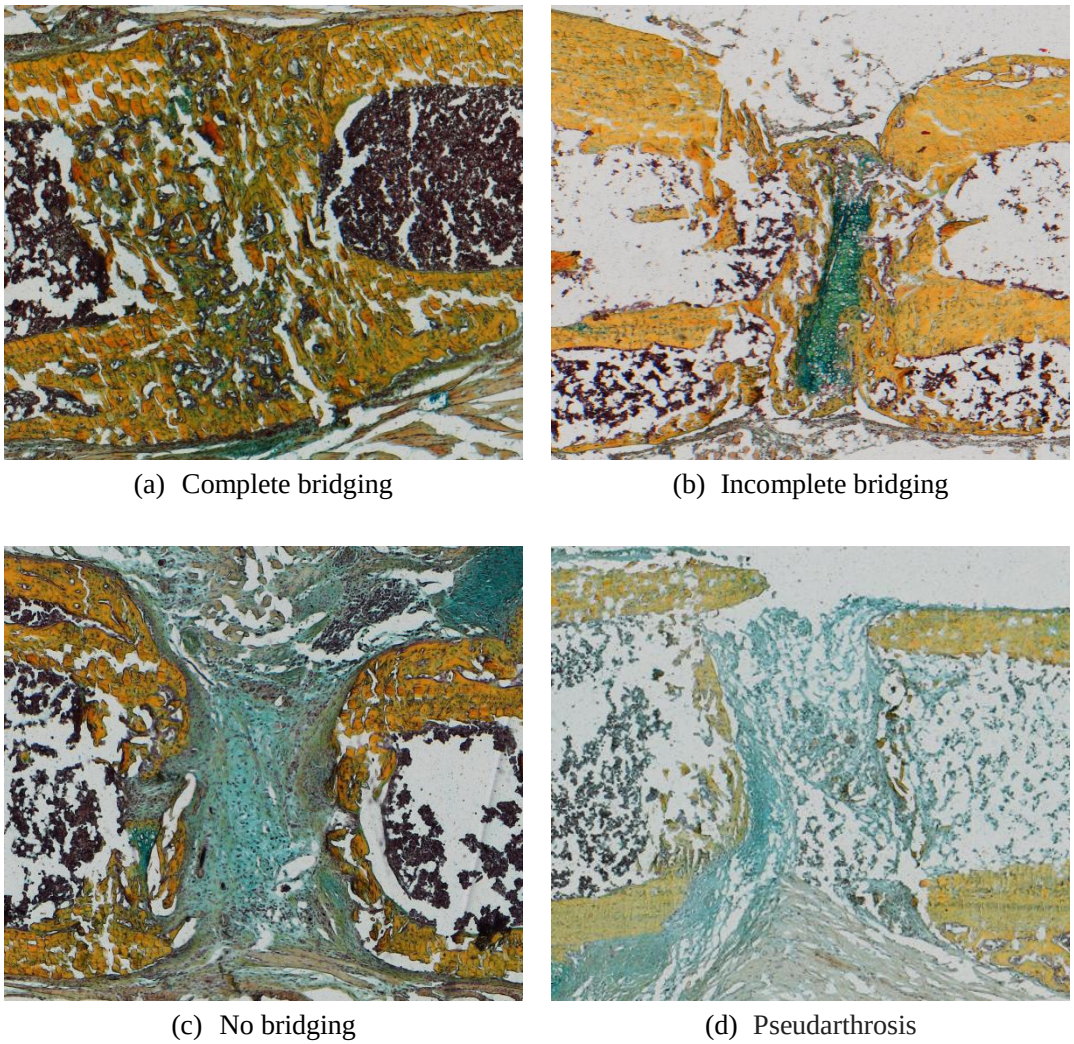

(a) Complete bridging (b) Incomplete bridging

(c) No bridging (d) Pseudarthrosis

Figure 7: Qualitative histomorphometric evaluation of fracture healing. A = complete bridging. B = incomplete bridging. C = no bridging. D = pseudarthrosis [67].

As for TRAP staining, a 1 mm wide ROI focused at fracture gap was chosen to draw the surface of osteoblasts and osteoclasts under the microscope at 20×magnification (Figure 10). The inclusion criteria for osteoblasts were: 1) grey cytoplasm, 2) flat shape, and 3) covering bone surfaces as lining cells. The inclusion criteria for osteoclasts were 1) two nuclei at least, 2) reddish brown cytoplasm, and 3) being adjacent to mineralized bone [68-71]. Two blinded and experienced reviewers

observed independently, and a third reviewer became involved when a large difference occurred. Meanwhile, the mineralized bone surface and the cellular surface were recorded by manual drawing. The cellular density was defined as the ratio of cellular surface and mineralized bone surface.

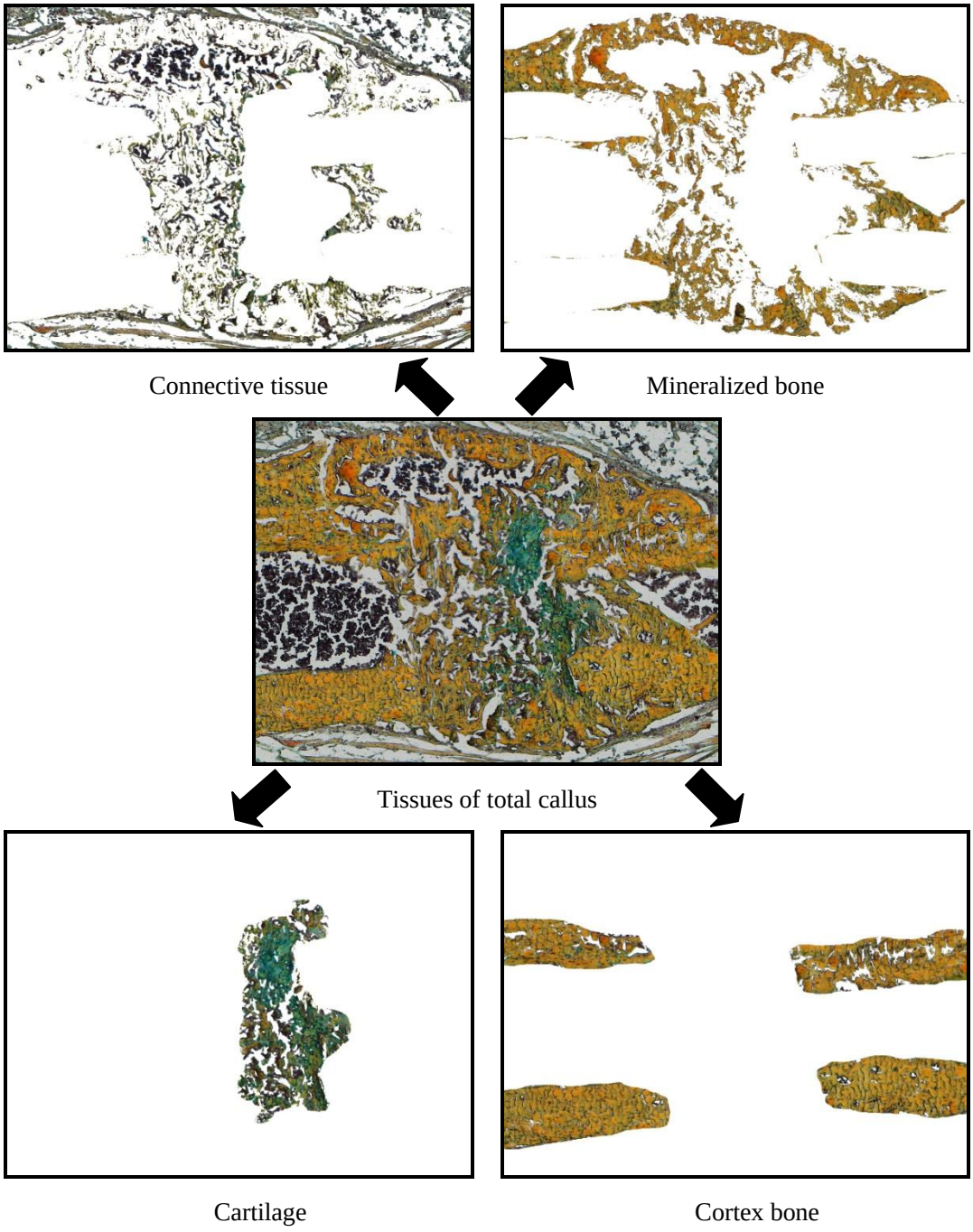

Figure 8: Quantitative histomorphometric evaluation of fracture healing. Callus of the ROI were divided into connective tissue, cartilage, mineralized bone and cortex bone with ImageJ. Areas of different components were calculated with ImageJ.

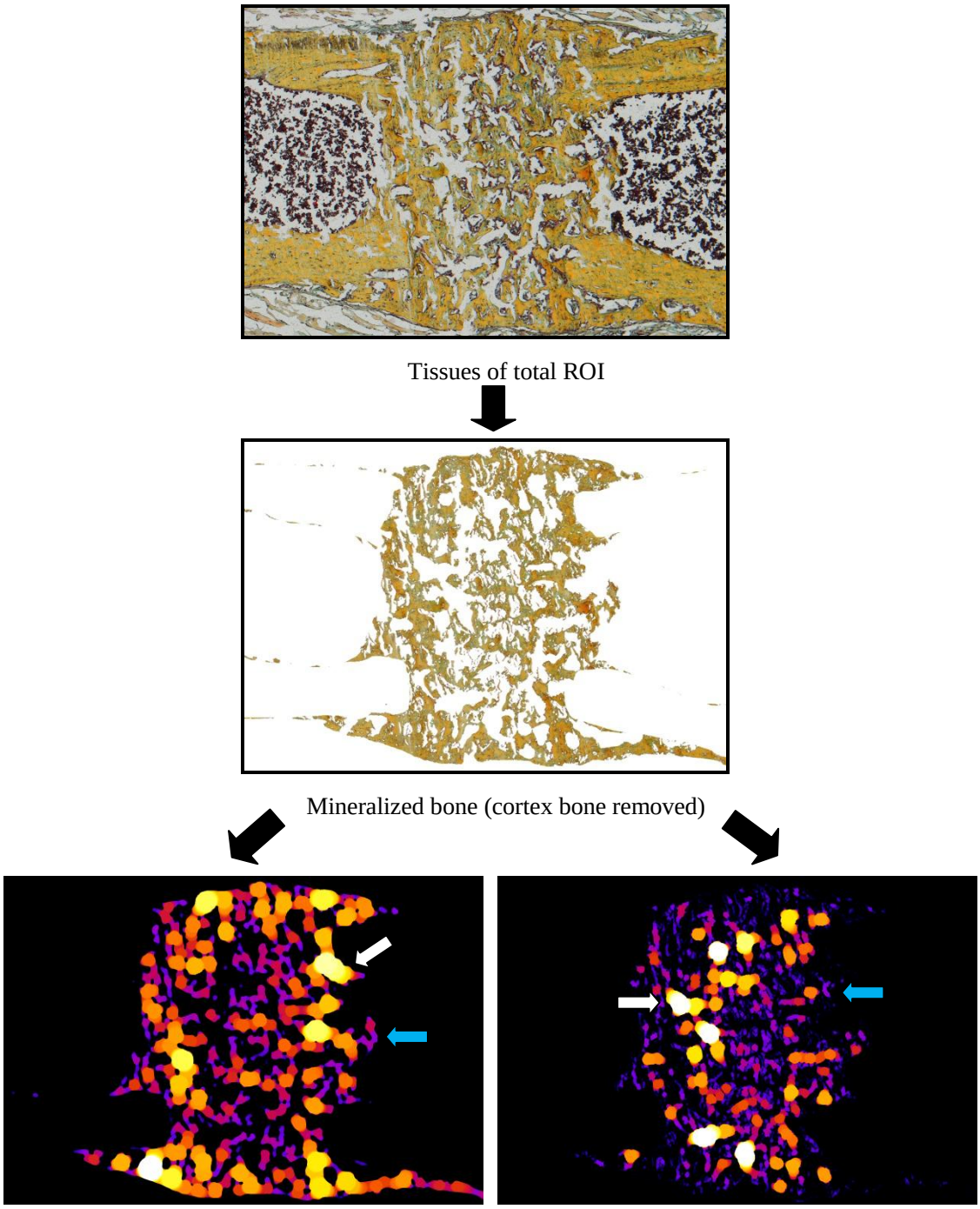

Figure 9: Trabecular bone score evaluation of callus microarchitecture. New forming mineralized bone was abstracted from the ROI of callus with ImageJ. The calculation of Tb.Th and Tb.Sp were carried out using ImageJ. The yellow dots (white arrow) represent higher value, while the purple dots (blue arrow) mean a lower value.

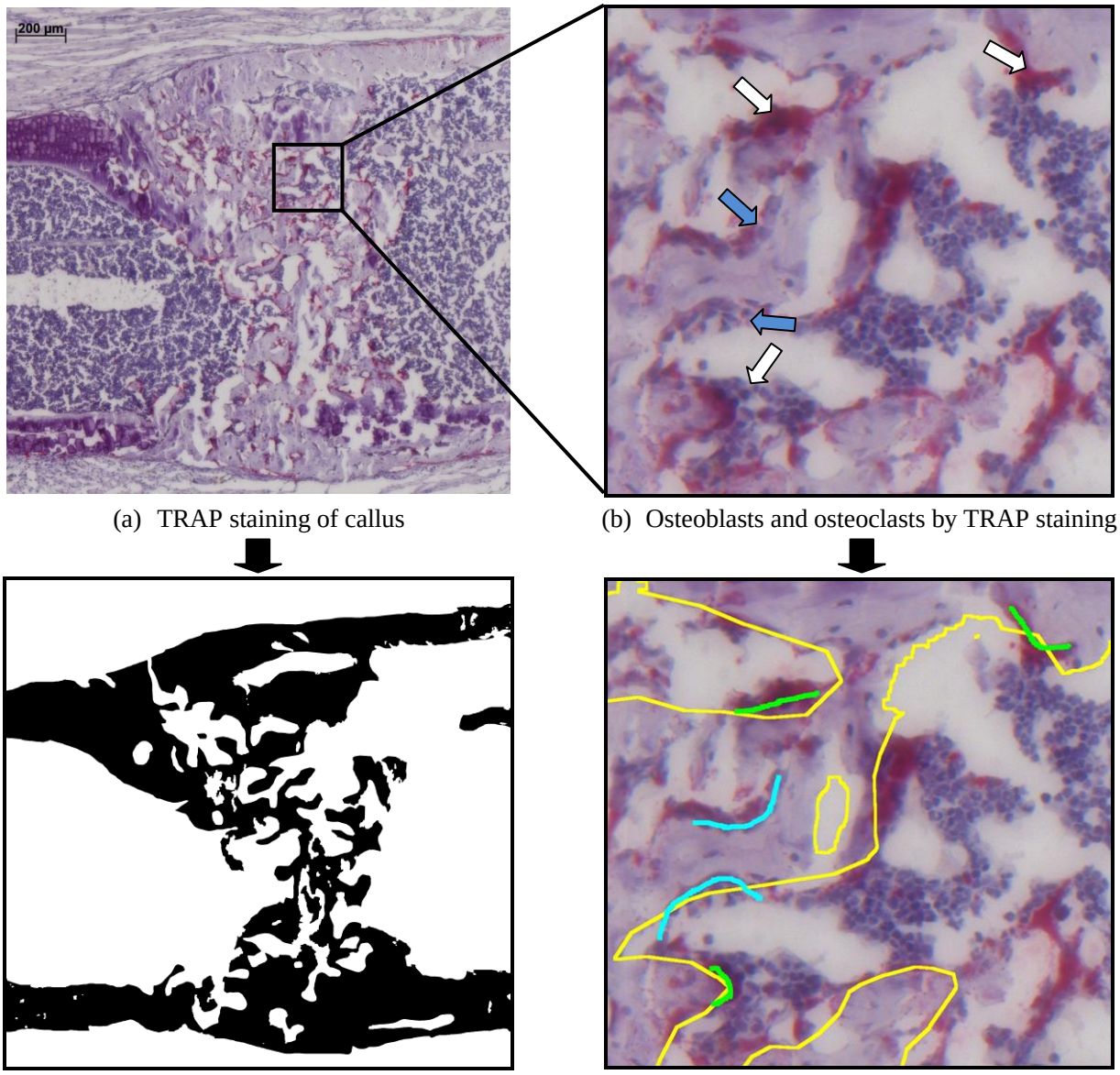

(a) TRAP staining of callus

(b) Osteoblasts and osteoclasts by TRAP staining

(c) Surface of mineralized bone

(d) Surfaces of osteoblasts and osteoclasts

Figure 10: Surface drawing of osteoblasts and osteoclasts. (a) TRAP staining of callus (1 mm wide). (b) osteoblasts (blue arrow) and osteoclasts (white arrow) with TRAP staining. (c) the surface of mineralized bone is presented by black shadow. (d) the surface of osteoblasts (blue line) and osteoclasts (green line). The surface of mineralized bone is shown by yellow line. The cellular density was defined as the ratio of cellular surface and mineralized bone surface.

2.5 Statistical analysis

Categorical variables (ABCD bridging score) were presented as percentages (%), while continuous variables were indicated as mean ± standard deviation and shown by box plots with median, 25th and 75th percentiles. Statistical evaluation of the data was performed using Stata (StataCorp LLC, Texas, USA). Data was tested for normality with the Kolmogorov-Smirnov test. Differences for categorical variables were assessed with the Fisher's exact test. For parametric variables, the Student's t-test was used for the comparison of two groups. Differences were considered statistically significant if the P value was < 0.05.

3 Results

3.1 Qualitative histomorphometric analysis

To evaluate the effect of TBI on fracture bridging in wild-type and ob/ob mice, the qualitative ABCD bridging score was presented as a percentage at week 3 and week 4 postoperation (Figure 11). The A and B scores were classified as bridged, while the C and D scores were defined as unbridged (Table 1). The Fisher's exact test was performed between bridged and unbridged categories.

In the wild-type mice, both fracture and fracture with TBI groups showed an increased bridging rate at week 4 compared with week 3. The fracture group showed a 55% complete bridging rate compared with 67% in the fracture with TBI group at week 3, and the corresponding comparison was 83% versus 80% at week 4, respectively. However, these differences were not statistically significant. In contrast, with ob/ob mice in contrast, the fracture group presented 70% pseudarthrosis and 30% no bridging, compared with 56% and 33% in the fracture with TBI group at week 3, and decreased slightly to 33% and 33% both in the fracture and the fracture with TBI groups at week 4. The the changes were not statistically significant, however.

However, both the fracture and the fracture with TBI group of ob/ob mice showed a significantly lower bridging rate compared with wild-type mice at week 3. The fracture group of ob/ob mice showed a 0% (A score + B score) bridged rate compared with 64% for wild-type mice ($p = 0.003$). Similarly in the fracture with TBI group, the ratio of bridged in the ob/ob mice was 11%, compared with 67% in the wild-type mice ($p = 0.02$). There were no statistical differences in the bridged rate at week 4 between the wild-type and the ob/ob mice in terms of the fracture and the fracture with TBI group.

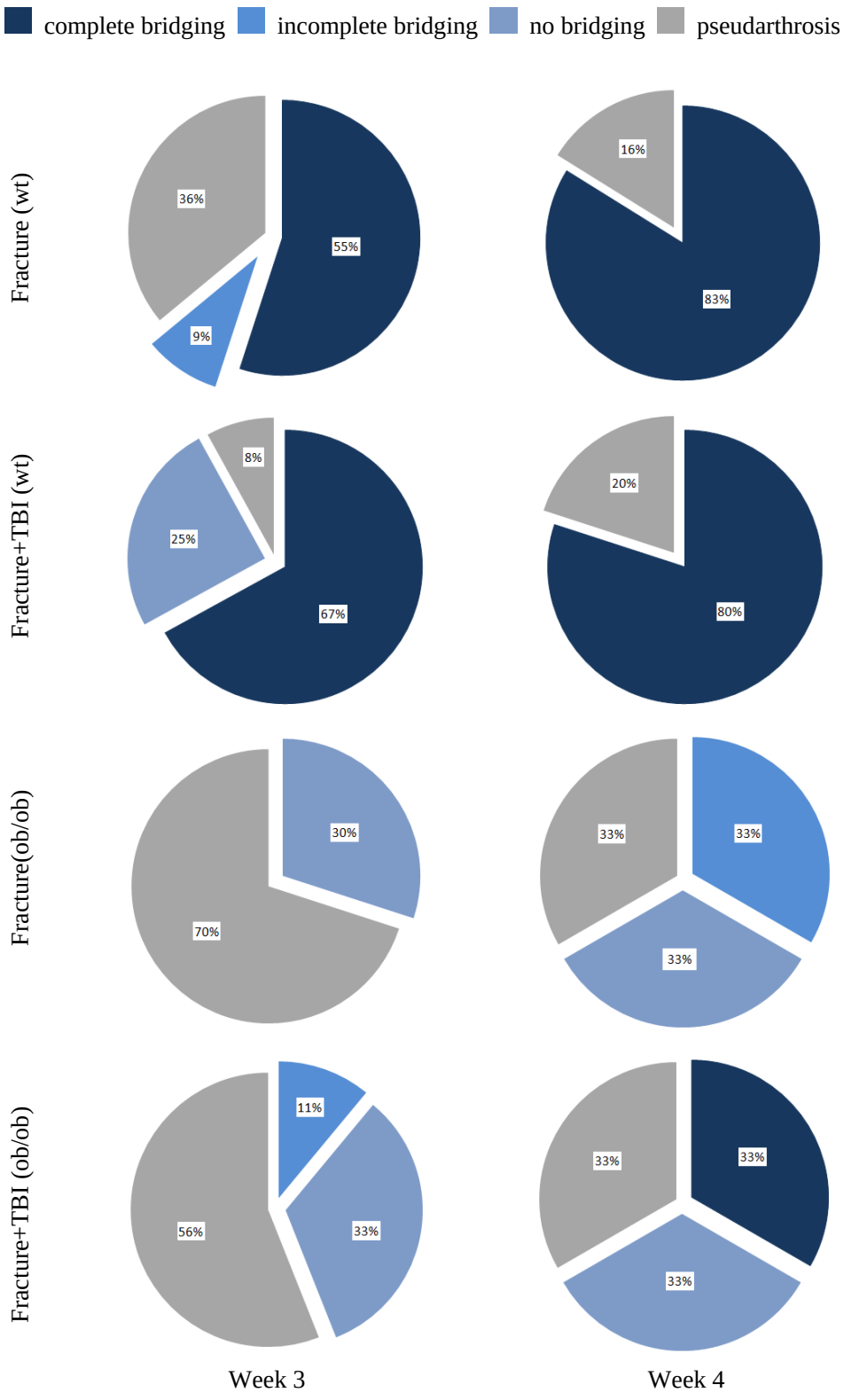

Figure 11: Results of qualitative evaluation of fracture bridging: the ratio of fracture healing classified as A, B, C or D score. A = complete bridging, B = incomplete bridging, C = no bridging and D = pseudarthrosis [67]. There were no significant differences between the fracture and the fracture with TBI group in the wild-type or the ob/ob mice (Fisher's exact test). However, both the fracture group ($p = 0.003$) and the fracture with TBI group ($p = 0.02$) of the ob/ob mice showed a statistically lower bridged rate compared with the wild-type mice at week 3.

		Week 3					Week4			
		A (%)	B (%)	C (%)	D (%)		A (%)	B (%)	C (%)	D (%)
Fracture (wt)	N=11	55	9	0	36	N=6	83	0	0	16
Fracture + TBI (wt)	N=12	67	0	25	8	N=5	80	0	0	20
Fracture (ob/ob)	N=10	0	0	30	70	N=6	0	33	33	33
Fracture + TBI (ob/ob)	N=9	0	11	33	56	N=6	33	0	33	33

Table 1: Results of qualitative evaluation of fracture bridging: the ratio of fracture healing classified as A, B, C or D. A = complete bridging, B = incomplete bridging, C = no bridging and D = pseudarthrosis [67]. In the Fisher's exact test, A + B = bridged and C + D = unbridged. There were no significant differences between the fracture and fracture with TBI group in wild-type or ob/ob mice. However, both the fracture group ($p = 0.003$) and fracture with TBI group ($p = 0.02$) of ob/ob mice showed a statistically lower bridging rate compared with the wild-type mice at week 3.

3.2 Quantitative histomorphometric analysis

3.2.1 Computed components of callus

Different components of the callus were abstracted with ImageJ. In the wild-type mice, it was found that the total MdBAr increased in the fracture with TBI group compared with the fracture group at week 4 ($p = 0.05$). In contrast, there was a decrease of total MdBAr in the fracture group at week 4 compared with those at week 3, although the difference was not statistically significant. In the ob/ob mice, the total MdBAr increased at week 4 compared with that of the fracture group in week 3 ($p = 0.003$), but there were no statistical differences between the fracture and the fracture with TBI group at week 3 or week 4 (Figure 12).

The wild-type mice showed a higher total MdBAr compared with the ob/ob mice, both in the fracture group ($p = 0.0001$) and in the fracture with TBI group ($p = 0.01$) at week 3. Moreover, total MdBAr was significantly increased in the wild-type mice compared with the ob/ob mice in the fracture with TBI group at week 4 (Table 2).

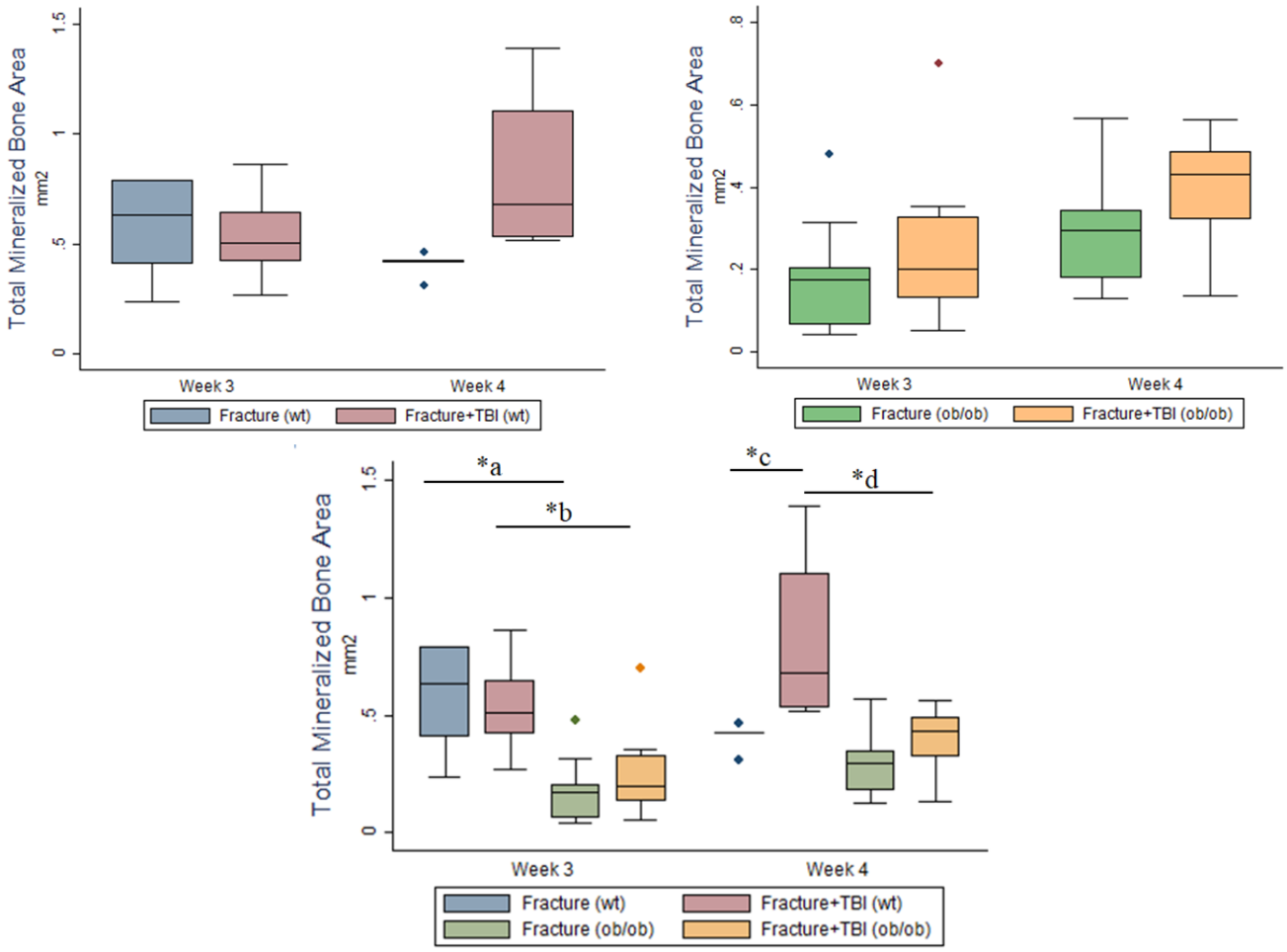

Figure 12: Results of total mineralized bone area. Results are shown by box plots with median, 25th and 75th percentiles. In the wild-type mice, the fracture with TBI group showed an increased total MdBAr compared with the fracture group at week 4. There were no significant differences between the fracture and the fracture with TBI group in the ob/ob mice at week 3 or 4. The wild-type mice presented higher total MdBAr compared with the ob/ob mice at week 3, both in the fracture and the fracture with TBI group, and at week 4 in the fracture with TBI group (* a p = 0.0001, * b p = 0.01, * c p = 0.05, * d p = 0.04).

Total MdBDn, which was defined as ratio of total MdBAr and total tissue area, was calculated (Figure 13). Similar to the total MdBAr, in the wild-type mice, the total MdBDn increased in the fracture with TBI group, compared with the fracture group at week 4 (p = 0.02). In the fracture group the MdBDn decreased from week 3 to week 4, although this tendency was not significant. In the ob/ob mice, total MdBDn did not show any significant differences between the fracture and the fracture with TBI group at week 3 or week 4.

The wild-type mice exhibited greater total MdBDn compared with the ob/ob mice, both in the fracture group (p = 0.001) and the fracture with TBI group (p = 0.01) at week 3. But in week 4, there were no significant differences in terms of total MdBDn in the fracture with TBI group between the wild-type and the ob/ob mice (Table 2).

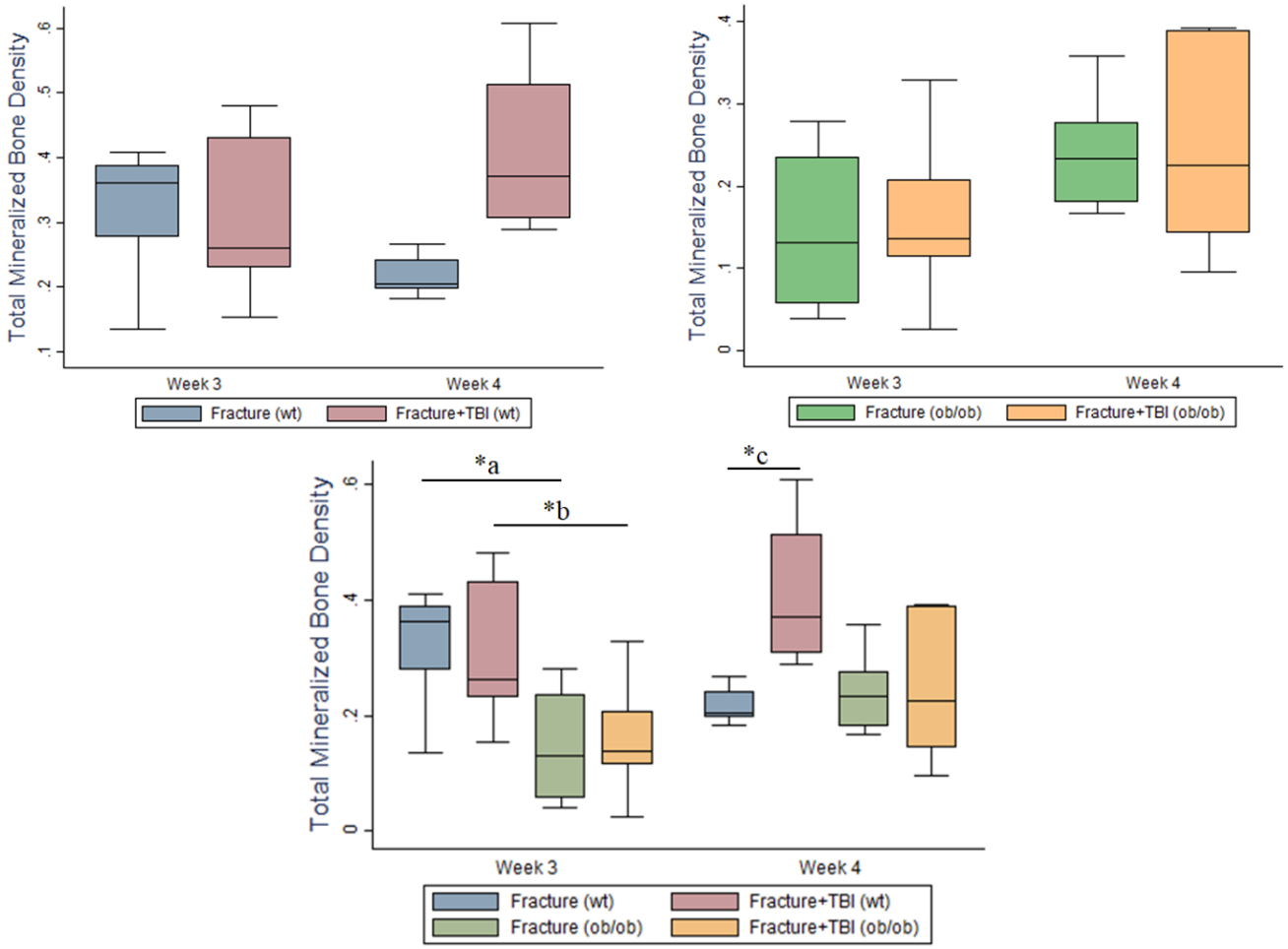

Figure 13: Results of total mineralized bone density. Results are shown by box plots with median, 25th and 75th percentiles. In wild-type mice, the fracture with TBI group showed increased total MdBDn compared with the fracture group at week 4. There were no significant differences between the fracture and the fracture with TBI group in the ob/ob mice at week 3 or 4. The wild-type mice presented higher total MdBDn compared with the ob/ob mice at week 3, both in the fracture and the fracture with TBI group (* a p = 0.001, * b p = 0.01, * c p = 0.02).

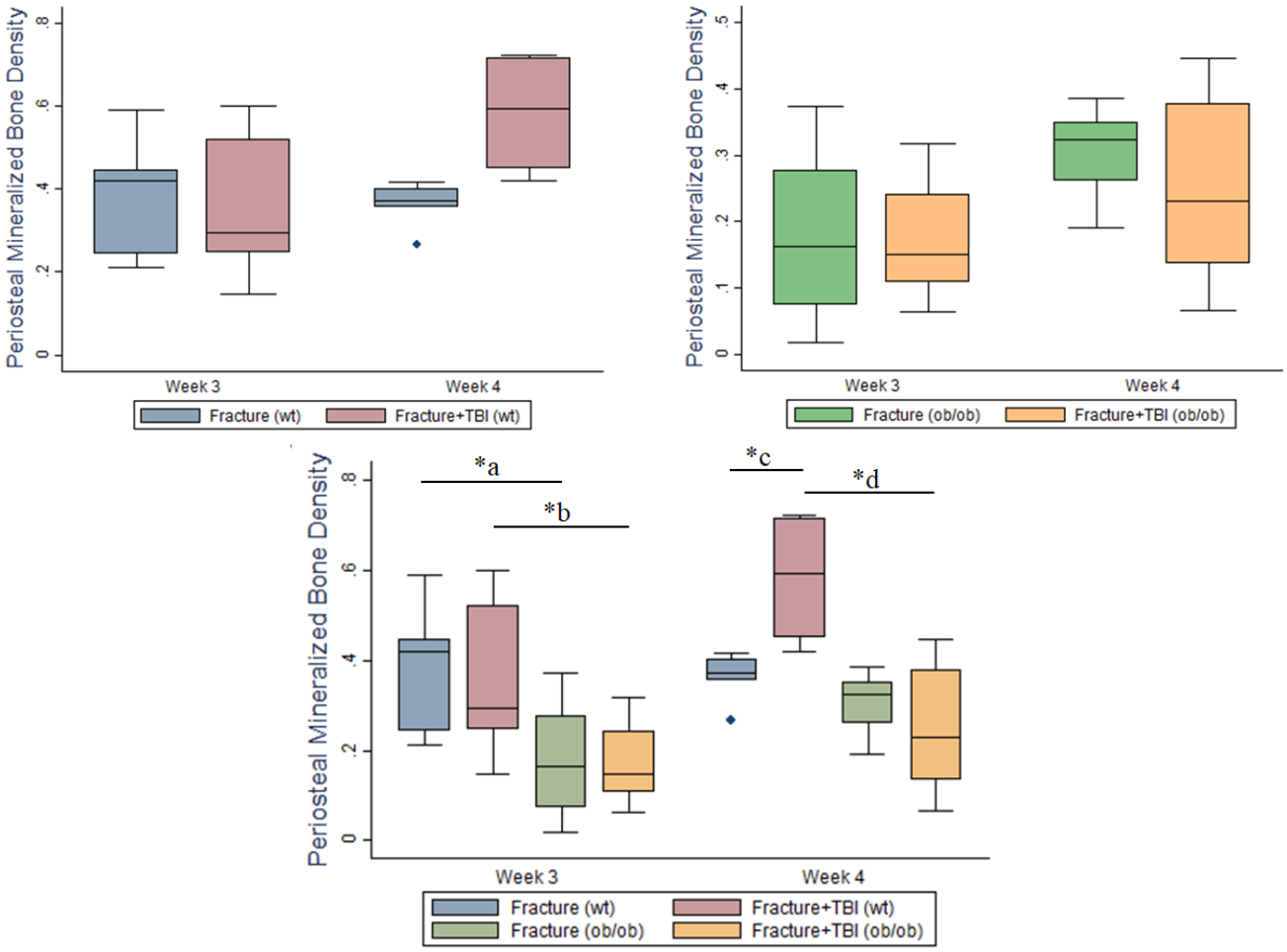

Figure 14: Results of periosteal mineralized bone density. Results are shown by box plots with median, 25th and 75th percentiles. In the wild-type mice, the fracture with TBI group showed increased periosteal MdBDn compared with the fracture group at week 4. The wild-type mice showed greater periosteal MdBDn compared with the ob/ob mice at week 3, both in the fracture and the fracture with TBI group, and at week 4 in the fracture with TBI group (* a $p = 0.005$, * b $p = 0.01$, * c $p = 0.02$, * d $p = 0.008$).

For better comparability, the periosteal and endosteal MdBDn were examined (Figures 14 and 15). For periosteal areas, the fracture with TBI group showed increased periosteal MdBDn compared with the fracture group at week 4 in the wild-type mice ($p = 0.02$). The fracture group presented higher periosteal MdBDn at week 4 compared with week 3 ($p = 0.01$) in the ob/ob mice. The wild-type mice showed greater periosteal MdBDn compared with the ob/ob mice both in the fracture and the fracture with TBI group at week 3, and in the fracture with TBI group at week 4.

Only a few significant differences were observed regarding the endosteal MdBDn. The fracture group in the wild-type mice showed higher endosteal MdBDn at week 3 compared with week 4 ($p = 0.02$). In the ob/ob mice, there were no significant differences in endosteal MdBDn between the fracture and the fracture with TBI group at week 3 or week 4. The wild-type mice had higher endosteal MdBDn compared with the ob/ob mice in the fracture group at week 3 only ($p = 0.007$) (Table 2).

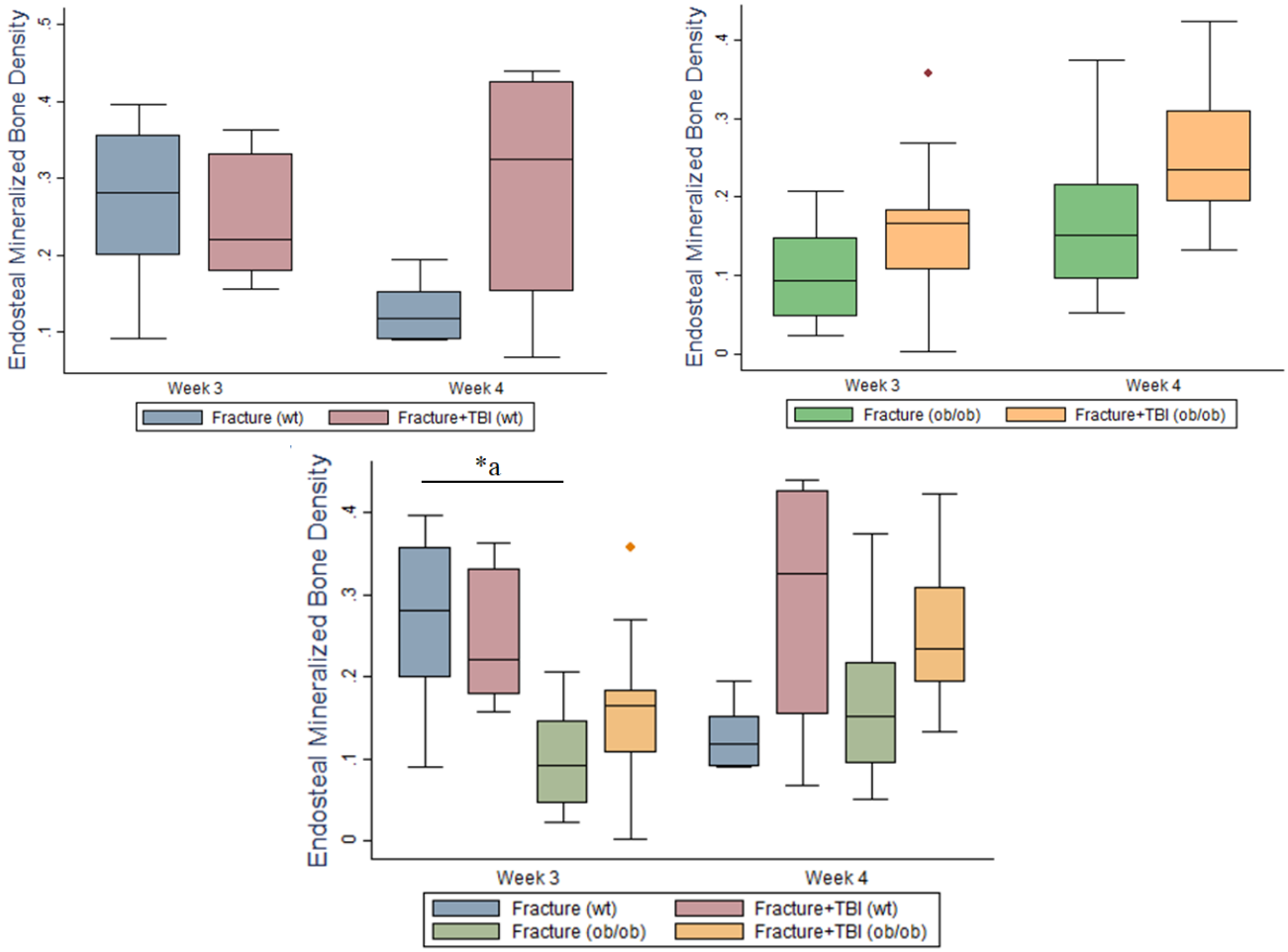

Figure 15: Results of endosteal mineralized bone density. Results are shown by box plots with median, 25th and 75th percentiles. In wild-type mice, only the fracture group showed increased endosteal MdBDn at week 4 compared with week 3 ($p = 0.02$). The wild-type mice exhibited higher periosteal MdBDn compared with the ob/ob mice at week 3 in the fracture group only (* a $p = 0.007$).

	Time point	Fracture					Fracture+TBI				
			wt		ob/ob	p value		wt		ob/ob	p value
Total Mineralized Bone Area(mm^2)	Week 3	N=11	0.58±0.20	N=10	0.17±0.13	0.0001	N=12	0.53±0.19	N=9	0.25±0.19	0.013
	Week 4	N=6	0.40±0.05	N=6	0.30±0.15	0.179	N=5	0.81±0.40	N=6	0.39±0.15	0.044
Total Mineralized Bone Density	Week 3	N=11	0.31±0.09	N=10	0.14±0.09	0.0016	N=12	0.30±0.11	N=9	0.16±0.09	0.014
	Week 4	N=6	0.21±0.03	N=6	0.24±0.07	0.527	N=5	0.40±0.14	N=6	0.24±0.12	0.088
Periosteal Mineralized Bone Density	Week 3	N=11	0.38±0.12	N=10	0.17±0.13	0.005	N=12	0.36±0.16	N=9	0.17±0.09	0.01
	Week 4	N=6	0.36±0.05	N=6	0.30±0.06	0.18	N=5	0.58±0.15	N=6	0.24±0.14	0.008
Endosteal Mineralized Bone Density	Week 3	N=11	0.26±0.10	N=10	0.10±0.06	0.0007	N=12	0.24±0.07	N=9	0.15±0.11	0.11
	Week 4	N=6	0.12±0.04	N=6	0.17±0.11	0.44	N=5	0.28±0.17	N=6	0.25±0.10	0.69

Table 2: Results of mineralized bone area and density. Results are shown by mean ± standard deviation. Bone area in mm^2 and bone density as percentage. N = sample size. The significant difference level of Student's t-test is $p < 0.05$.

3.2.2 Trabecular bone score of callus

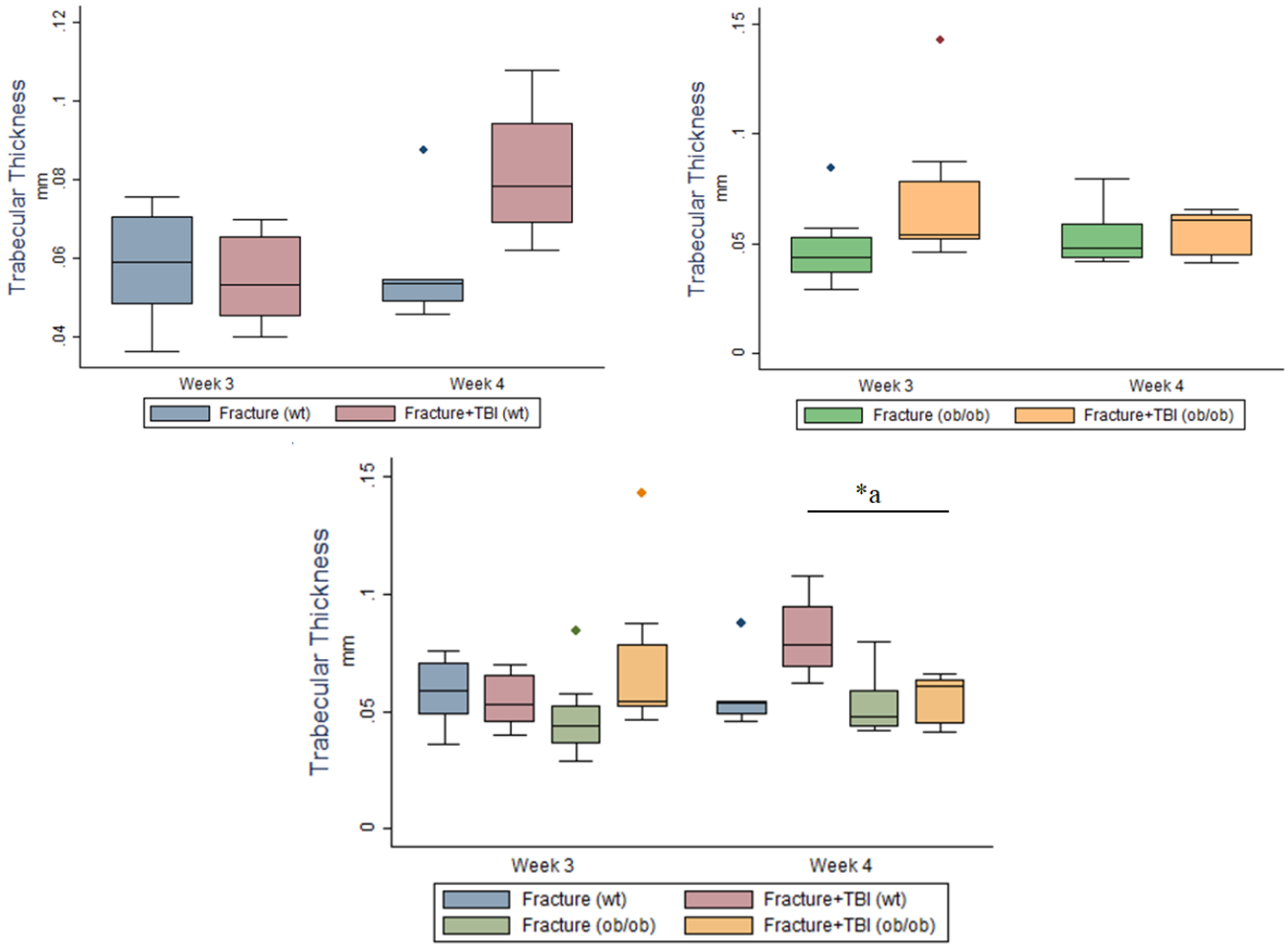

Figure 16: Results of trabecular thickness. Results are shown by box plots with median, 25th and 75th percentiles. There were no significant differences of Tb.Th in the ob/ob mice between the fracture and the fracture with TBI group at any observed time points. The ob/ob mice showed lower Tb.Th compared with the wild-type mice in the fracture with TBI group at week 4 (* a p = 0.02).

Trabecular bone score based on micro-CT has been widely applied in describing the three dimensional microarchitecture of bone callus. In this study, trabecular thickness (Tb.Th) and separation (Tb.Sp) were examined on two dimensional Movat staining slices with ImageJ. In the wild-type mice, the fracture with TBI group presented higher Tb.Th at week 4 compared with week 3 ($p = 0.01$). In ob/ob mice, no significant differences of Tb.Th were observed between the fracture and the fracture with TBI group at week 3 or week 4. The ob/ob mice showed lower Tb.Th compared with the wild-type mice in the fracture with TBI group at week 4 ($p = 0.02$) (Figure 16).

In terms of Tb.Sp, the only statistically significant difference was found in the wild-type compared with the ob/ob mice in the fracture with TBI group at week 4 (p = 0.007). Neither the wild-type nor the ob/ob mice presented significant differences of Tb.Sp between the fracture and the fracture with TBI group at week 3 or week 4 (Figure 17, Table 3).

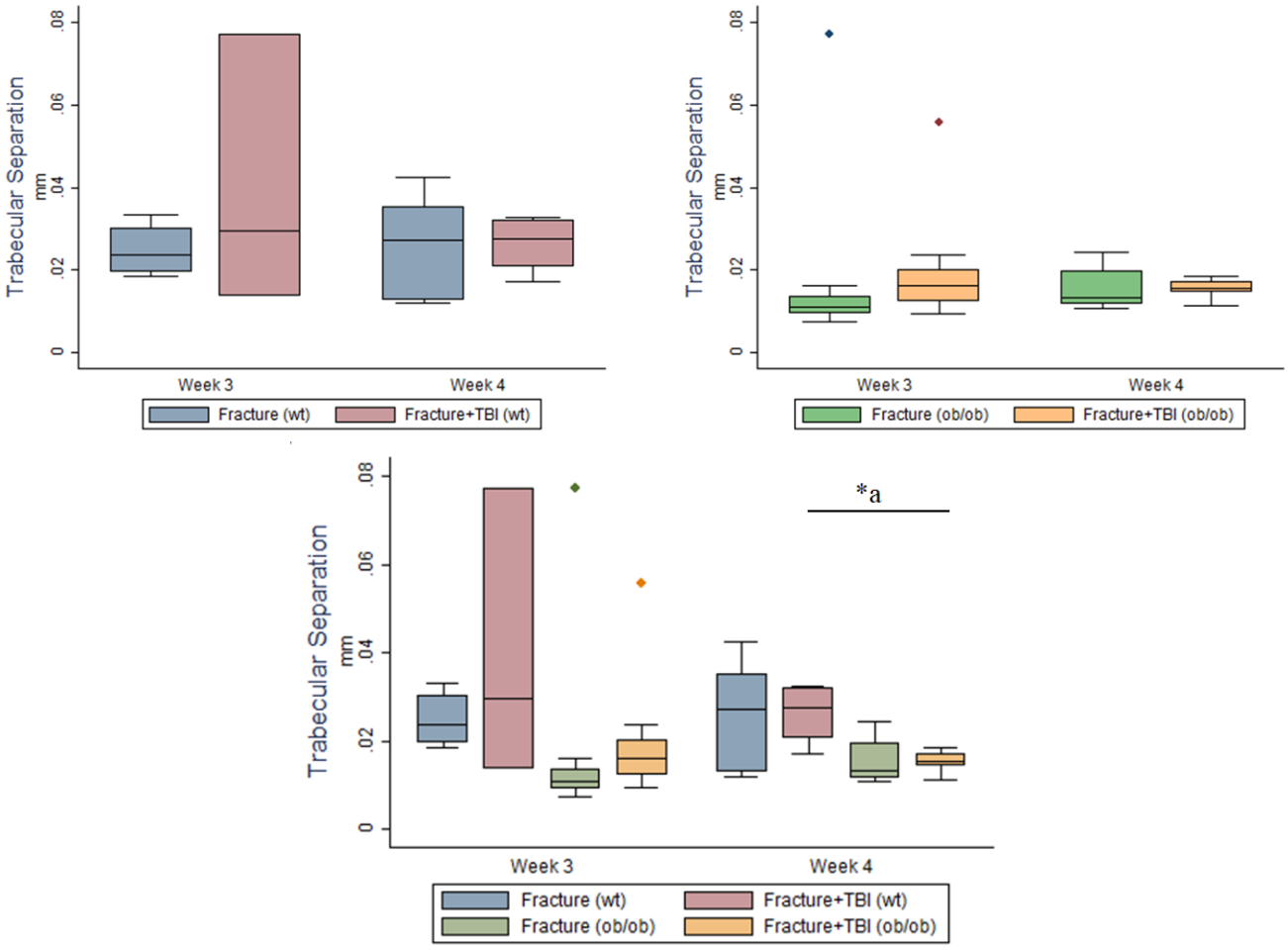

Figure 17: Results of trabecular separation. Results are shown by box plots with median, 25th and 75th percentiles. There were no significant differences of Tb.Sp between the fracture and the fracture with TBI group at week 3 or week 4 in the wild-type mice. The same applied with the ob/ob mice. A statistical difference was found in the wild-type compared with the ob/ob mice in the fracture with TBI group at week 4 (* a p = 0.007).

	Time point		Fracture				Fracture+TBI				
			wt		ob/ob	p value		wt		ob/ob	p value
Trabecular Thickness(mm)	Week 3	N=11	0.058±0.013	N=10	0.047±0.015	0.14	N=12	0.054±0.010	N=9	0.069±0.030	0.25
	Week 4	N=6	0.058±0.016	N=6	0.053±0.014	0.60	N=5	0.081±0.019	N=6	0.056±0.010	0.02
Trabecular Separation(mm)	Week 3	N=11	0.025±0.006	N=10	0.017±0.021	0.38	N=12	0.023±0.004	N=9	0.020±0.014	0.57
	Week 4	N=6	0.026±0.013	N=6	0.015±0.005	0.11	N=5	0.026±0.007	N=6	0.015±0.002	0.002

Table 3: Results of trabecular thickness and separation. Results are shown by mean ± standard deviation. Trabecular thickness and separation in mm. N = sample size. The significant difference level of Student's t-test is $p < 0.05$.

3.2.3 Cellular density analysis

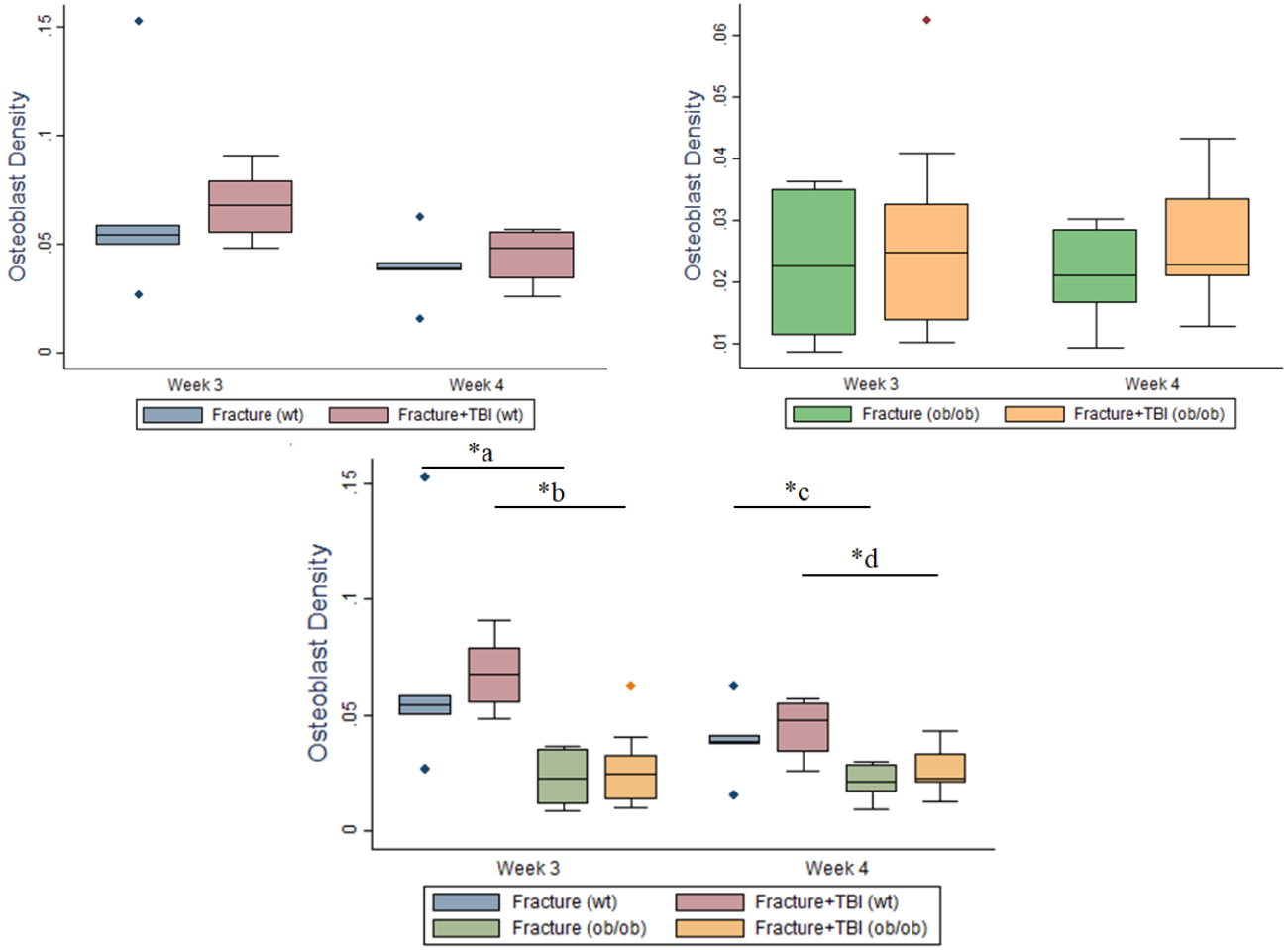

Figure 18: Results of osteoblast density. Results are shown by box plots with median, 25th and 75th percentiles. There were no statistical differences between the fracture and fracture with TBI group at week 3 or week 4 in the ob/ob mice. However, the wild-type mice showed higher osteoblast density compared with ob/ob mice both in the fracture group and the fracture with TBI group at week 3 as well as week 4. (* a p = 0.006, * b p = 0.0001, * c p = 0.04, * d p = 0.04).

To understand the proliferation of cells during fracture healing influenced by TBI in the wild-type and the ob/ob mice, osteoblast and osteoclast densities, which were defined as the cellular surface divided by total mineralized bone surface, were recorded by manual drawing in ImageJ.

In the wild-type mice, osteoblast density at week 4 decreased compared with week 3 in the fracture with TBI group (p = 0.02), While in the ob/ob mice, there were no statistical differences between the fracture and the fracture with TBI group at week 3 or week 4. The wild-type mice, however, showed higher osteoblast density compared with the ob/ob mice, both in the fracture group (p = 0.006) and the fracture with TBI

group (p = 0.001) at week 3 as well as week 4 (fracture group: p = 0.04, fracture with TBI group: p = 0.04) (Figure 18).

There were no significant differences of osteoclast density in the wild-type mice between the fracture and the fracture with TBI group at week 3 or week 4 (Figure 19). Moreover, no statistically significant differences were found in each group of the ob/ob mice at all observed time points. As was observed for the osteoblast density, the wild-type mice exhibited higher osteoclast density than the ob/ob mice at each time point (week 3: fracture group: p = 0.02, fracture with TBI group: p = 0.02; week 4: fracture group: 0.04, fracture with TBI group: p = 0.005) (Table 4).

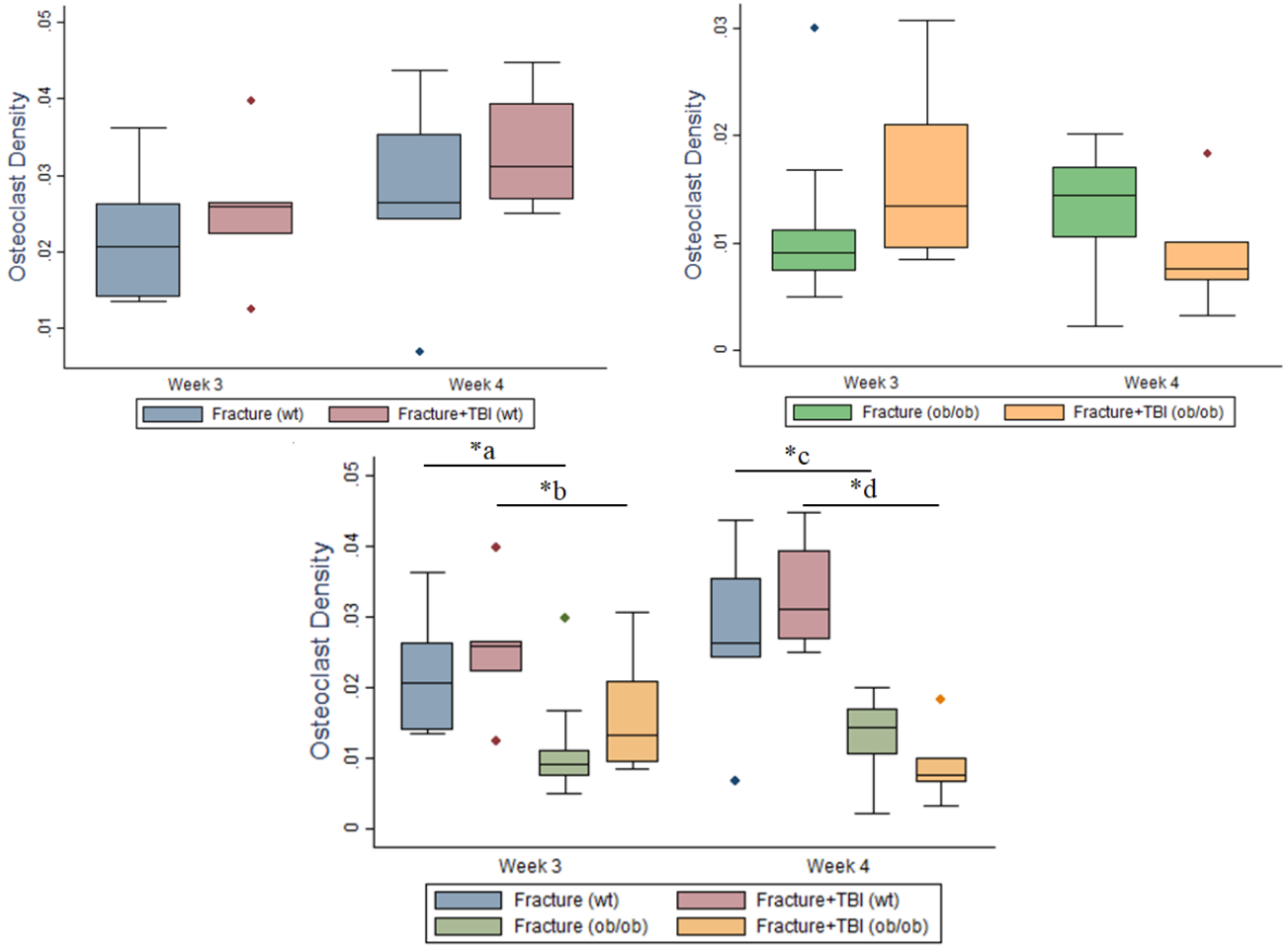

Figure 19: Results of osteoclast density. Results are shown by box plots with median, 25th and 75th percentiles. No statistical differences were observed between the fracture and the fracture with TBI group at week 3 or week 4 in the wild-type mice. The same applied to the ob/ob mice. The wild-type mice showed higher osteoclast density than the ob/ob mice in the comparable group at each time point. (* a p = 0.02, * b p = 0.02, * c p = 0.04, * d p = 0.005).

	Time point	Fracture					Fracture+TBI				
		wt		ob/ob		p value	Wt		ob/ob		p value
Osteoblast Density	Week 3	N=11	0.064 ± 0.040	N=10	0.022 ± 0.011	0.006	N=12	0.068 ± 0.014	N=9	0.027 ± 0.016	0.0001
	Week 4	N=6	0.039 ± 0.016	N=6	0.021 ± 0.007	0.04	N=5	0.044 ± 0.014	N=6	0.026 ± 0.010	0.04
Osteoclast Density	Week 3	N=11	0.021 ± 0.008	N=10	0.011 ± 0.007	0.02	N=12	0.025 ± 0.008	N=9	0.015 ± 0.007	0.02
	Week 4	N=6	0.027 ± 0.013	N=6	0.013 ± 0.006	0.048	N=5	0.033 ± 0.008	N=6	0.009 ± 0.005	0.005

Table 4: Results of osteoblast and osteoclast density. Results are shown by mean ± standard deviation. Osteoblast and osteoclast density as percentage. N = sample size. The significant difference level of Student's t-test is $p < 0.05$.

4 Discussion

4.1 Histomorphometric validation of the effect of TBI on fracture healing

In the wild-type mice, the fracture with TBI group showed increased callus formation at week 4. Our findings were consistent with published experimental studies [11-19]. Boes *et al.* [18] demonstrated that TBI increased bone stiffness during fracture healing. In addition, Song *et al.* [19] described the increased BMD and BMC of the callus in the fracture with TBI group by micro-CT in SD rats. In the studies of Wei and Wang [55, 56], the callus diameters of intramedullary fixated femoral fractures in rats were assessed in conventional x-rays with the use of the Perkins volume formula [16]. The authors reported an increase in callus volume in the combined trauma group up until week 8. Maegele *et al.* used a rat neurotrauma model and performed an *ex vivo* histomorphometric evaluation of newly-formed callus in non-fixated tibia fractures after implant removal. Similarly to our findings, the authors demonstrated the remarkably increased callus mass in the combined trauma group at two weeks after trauma [72].

However, our study indicated there were no significant differences between the fracture and the fracture with TBI groups at week 3 concerning total MdBAr and MdBDn. Our micro-CT results showed an increase in the bone volume following TBI [73]. Since histomorphometry allows only two dimensional analyses, the three dimensional micro-CT seems more reliable. Moreover, the ABCD bridging score reported in the fracture and the fracture with TBI groups showed no significant difference. Considering the high bridged rate, it could be speculated that an earlier observation time point would be needed to evaluate the bridging situation.

Meanwhile, in order to clarify the location and distribution of bone formation, we

calculated the periosteal and endosteal MdBDn. Interestingly, the fracture with TBI group presented higher periosteal MdBDn, which could be attributed to two reasons. On one hand, there could be more intensive callus formation triggered by TBI. On the other hand, the callus remodeling in the group with fracture and TBI could be delayed. There was no significant difference in the endosteal MdBDn, which could be explained by the progressed resorption of the endosteal callus by osteoclasts. This was in line with the high ABCD bridging score, representing an advanced healing process.

Furthermore, the trabecular bone score was recorded in order to measure the quality of callus. Due to the limitations of two-dimensional histomorphometry, only trabecular thickness and separation were obtained. No significant differences were detected between the fracture and the fracture with TBI groups, which indicated that TBI did not have an impact on the architecture of trabeculae.

Unexpectedly, osteoblast and osteoclast density were not affected by TBI. These findings were not consistent with previous *in vitro* reports. Cadosch and Gautschi *et al.* [11, 12, 22] found that the serum and CSF from patients with TBI combined femoral fracture significantly accelerated the proliferation rates of human foetal osteoblastic cell and osteoblast cultures. Boes *et al.* [18] showed that the serum of rats with fracture and TBI exhibited a significantly higher osteoinductive potential for the proliferation of MSC cultures than serum from rats with an isolated fracture. Yang *et al.* [29] showed that the serum from TBI rats promoted the proliferation of osteoblastic MC3T3-E1 cells. This discrepancy could be attributed to the differing environments between *in vivo* and *in vitro* experiments.

4.2 The compromised fracture healing in ob/ob mice

Compared with the wild-type mice, the ob/ob mice presented a significantly lower ABCD bridging score at week 3. While the fracture group of the wild-type mice exhibited a high rate of bridging, all of the ob/ob mice in the fracture group showed either no bridging or pseudarthrosis. Moreover, the ob/ob mice showed decreased

total MdBAr and MdBDn, as well as periosteal and endosteal MdBDn, compared with the wild-type mice at week 3. These outcomes, in accordance with the radiological findings of our group [74], provided evidence that the ob/ob mice showed compromised fracture healing, and confirmed the crucial role of leptin on bone formation. However, there were no statistical differences between the wild-type and ob/ob mice in terms of trabecular thickness and separation, which implied that leptin may not be able to influence the architecture of callus in fracture healing.

There is mixed evidence in the existing literature in this regard. Beil *et al.* [75] observed increased periosteal callus formation and earlier mineralization in the ob/ob mice. Yue *et al.* [52] chose Prx1-Cre; $Lepr^{fl/fl}$ mice whose leptin receptor was conditionally deleted from MSCs of the extremities, but not from the axial skeleton or CNS, in order to explore the direct peripheral influence of leptin. They found that the $Lepr^{fl/fl}$ mice showed higher bone volume, trabecular number and thickness in fracture callus. Contrarily, Rőszer *et al.* [76] described a deleterious effect of leptin receptor deficiency in fracture healing by histology and micro-CT. Khan *et al.* [77] reported that the ob/ob mice showed increased callus volume compared to the wild-type mice by micro-CT, but the callus was predominantly hypertrophic and unmineralized cartilage. These discrepancies could be attributed to: 1) different signal pathways of ob/ob and leptin receptor deficiency mice models; 2) differences among the fracture models, such as guillotine and osteotomy; 3) diverse means of fixation, for instance, intramedullary nailing and external fixation.

As to the cellular proliferation, we assessed the osteoblast and osteoclast densities which were defined as the ratios of cellular surface and total mineralized bone surface in order to avoid bias due to differences of mineralized bone surface [68]. The outcomes showed that the ob/ob mice presented lower osteoblast and osteoclast density than the wild-type mice at week 3 and week 4. Some previous studies support this finding. Gordeladze *et al.* [53] showed that leptin resisted the apoptosis of osteoblasts and induced the differentiation of osteoblasts into osteocytes. Thomas *et al.*

[54] found that leptin augmented the differentiation of MSCs into osteoblasts and inhibited differentiation into adipocytes. Turner *et al.* [50] emphasized the reduction in the activity of osteoblasts, and increase in the activity of osteoclasts, in the normal femoral diaphysis of the ob/ob mice, which could be due to the different processes involved in bone metabolism and fracture healing. Yet Yue *et al.* [52] showed that peripheral leptin receptor signaling promoted adipogenesis and inhibited osteogenesis by MSCs, while deletion of leptin receptor in osteoblasts could not affect osteogenesis or adipogenesis. Therefore, leptin affects bone development and metabolism through hypothalamus-β-adrenergic receptor and direct peripheral receptors. Peripheral leptin had a negative effect on fracture healing in Yue's article.

4.3 Leptin-deficiency and TBI

Comparing the fracture and fracture with TBI groups in the ob/ob mice, we provided evidence that leptin-deficiency eliminated the positive effect of TBI on fracture healing. The results hold not only in terms of the ABCD bridging score, but also MdBAr and MdBDn. There were no remarkable differences between the two groups in those measurements. These findings were consistent with the radiological results of our group [74], and they indicated that leptin plays an important role in the interaction between TBI and accelerated fracture healing.

Wang *et al.* [55] reported higher concentrations of leptin in the serum of the TBI with fracture group compared with that of groups with isolated injuries. Furthermore, Wei *et al.* [56] reported that the leptin in serum significantly increased in the fracture, TBI and the fracture with TBI groups compared with the control group. In a clinical study, Lin *et al.* [57] found that the serum leptin level in the fracture with TBI patients was substantially higher than that of the control group. Yan et al [34] explored the role of leptin on fracture healing after TBI with rabbits and reported the following: 1) higher leptin in serum and CSF in the TBI group than that in the sham-operation group; 2) the cerebellomedullary cistern injection of leptin promoted fracture healing; 3) the

Fluorescence-leptin was detected in brain of TBI; and 4) PCR showed no significant differences between the TBI and sham-operated animals regarding the autocrine of leptin in the brain. The series of results indicated leptin played a positive role in fracture healing with TBI through the central signal pathway.

Similarly to the results on fracture healing in the ob/ob mice, TBI did not improve the osteoblast and osteoclast density in the ob/ob mice. As described above, TBI did not augment the osteoblast and osteoclast density of the wild-type mice in fracture healing, which suggested that the positive effect of TBI on fracture healing did not rely on proliferation, but rather on the enhanced cellular function. Meanwhile, lower osteoblast and osteoclast density were found in the fracture healing of the ob/ob mice compared to the wild-type animals. As the inverse relationship between adipogenesis and osteogenesis in MSCs is widely accepted [78-81], the factors that promoted MSC adipogenic differentiation were effective at the expense of osteogenesis and vice versa. A reasonable conjecture could be the ob/ob mice exhibited a dysplasia of osteoblast proliferation that could not be improved by additional TBI.

4.4 Selection of experimental animals and traumatic models

In clinical practice, different traumatic patterns with additional injuries presented with complicated healing processes, which can disturb the evaluation of fracture healing after TBI. Therefore, standardized animal models of fracture and TBI are necessary in order to identify the influence of TBI on fracture healing, and elucidate the underlying mechanism of the acceleration of fracture healing after TBI.

The mouse was chosen as our experimental animal, primarily because it would be immediately comparable to the existing literature. The ob/ob mouse has been widely used in the research of bone development and metabolism, and as such, comparisons between our results and previous works allowed better understanding of the relevant underlying mechanisms. Moreover, the mouse was chosen as it is cheaper to purchase and house than other animals, such as the rabbit and the sheep [82]. In addition, due to

the widely explored mouse genome, it is possible to clarify the molecular mechanisms of fracture healing with TBI by gene expression studies and in genetically modified mice [83].

Nonetheless, mouse models have certain drawbacks. The surgical techniques with small mice are quite complicated [82]. Also, the differences of bone architecture between mice and human have to be noted. The lamellar bone of mice contains primary osteons instead of Havers systems [83]. Weighing the pros and cons, mouse models are still excellent animal models for fracture healing studies.

Unlike intramedullary nailing and locking plates, external fixators have no contact with the osteotomy gap and therefore can minimize the disturbance of the callus formation. The convenient removal of the external fixator can maintain the intactness of samples during organ harvest. The rigid external fixator showed high stiffness, with axial and rotational stability in fracture healing [82]. The rigid stability was indispensable for fracture healing in the ob/ob mice, since different loading on the fracture gap led to distinct interfragmentary movements (IFMs), resulting in diverse callus formations [85-87]. Considering the higher body weight of the ob/ob mice, it was reasonable to assume that mechanical load caused by instability induced higher IFMs in the fracture gap than that in the wild-type mice. The stability of fracture induced by the rigid external fixator limited IFMs, and therefore minimized the influence of different body weights on fracture healing between the wild-type and the ob/ob mice.

The fracture model applied in this study was performed as osteotomy with a bone defect of 0.7 mm. According to the consensus on fracture models of small animals, it was recommended that the osteotomy gap in open fracture should not exceed 20% of the bone diameter [82]. The diameters of femoral diaphyses of mice adopted in our study were 1.4-2.0 mm, resulting in a suitable bone defect width of 0.28-0.4 mm. The 0.7 mm bone defect leads to a larger fracture gap, which enables a better exploration of the details of fracture healing through the prolonged healing process. Although the

0.7 mm osteotomy gap might be responsible for the high percentage of incomplete bridging in the ob/ob mice at week 3 and also week 4, the wild-type mice showed a high percentage of complete bridging with a 0.7 mm bone defect at week 3.

TBI is diversely classified based on, for example, severity and location among other factors, which results in complicated pathologic mechanisms, such as focal contusion, cerebral edema, intracranial hemorrhage, perfusion disorder and mechanical nerve fiber damage [62]. Thus, the standardized TBI model was required to evaluate the influence on fracture healing. In this experiment, TBI was produced by a standardized controlled cortical impact (CCI) device which was performed at our institute after craniotomy [62, 88]. After TBI was induced by CCI, pathophysiological procedures of cortical contusion, axonal damage, concussion, and damage of blood brain barrier (BBB) were followed [61, 89, 90]. The pneumatic CCI device was operated automatically, after operating parameters (including firing pin diameter, impact angle, penetration depth, impact speed and contact duration) were set. Therefore, the severity and location of TBI were standardized by the defined operating parameters of the CCI device. In addition, the CCI device provided reproducible and comparable TBI models, while other TBI models, such as weight drop model, cortical cold lesion and the fluid percussion model, are not easily standardized and repeated [91].

4.5 Evaluation of fracture healing by histomorphometry

The evaluation of fracture healing in this study was performed by qualitative and quantitative histomorphometry. Histological analysis has been widely applied for the evaluation of facture healing with several advantages over micro-CT. Firstly, it is vitally important to observe cellular processes. As such, it was made possible to assess osteoblast and osteoclast density in the present work. Additionally, analyses of different components of the callus were able to be carried out, while conversely, micro-CT would have only categorized the calcified tissue and non-calcified tissue by tissue density. However, the pitfalls of histological analysis were still presented. With

micro-CT analysis, three-dimensional reconstruction accurately exhibited the volume of the callus, while histological analysis could only produce two-dimensional evaluation [73, 74, 92]. The results for the callus volume from micro-CT presented distinct accuracy compared to histological analysis in fracture healing. Moreover, by *in vivo* micro-CT assay, noninvasive scans created long-term and continuous observations, and therefore time series evaluations of the dynamic processes of fracture healing could be possible [73, 74, 93]. Lastly, samples for histological analysis must be harvested after the sacrifice of animals, which means more time series' of observations are required. Hence, more animals and higher experimental costs are expected. Nevertheless, histological evaluation was essential for the elucidation of the molecular mechanisms of fracture healing given its irreplaceable advantages, which is also the consensus of studies on small animal bone healing models [82].

Qualitative and quantitative histomorphometry are applied widely for the evaluation of fracture healing. The qualitative histomorphometric analysis was performed with the use of the ABCD bridging score. Due to the characteristics of fracture healing, the bone absorption at the callus remodeling stage occurred at the terminal stage of the fracture healing process. MdBAr and MdBDn do not always measure the ongoing healing process, because at late healing stages, the callus is resorbed. Therefore, the combined evaluation of the ABCD bridging score, and MdBAr and MdBDn is much more reliable for verifying the entire process of proper healing [73, 74].

MdBAr was the main indicator for the quantitative histomorphometric assessment of fracture healing [71, 94]. Due to the uncertain calibration of histological cutting from the medial axis of the femora, MdBDn, which was defined as the ratio of MdBAr and total tissue area, was applied to minimize possible biases [94]. Moreover, MdBDn was calculated in the periosteal and endosteal areas separately, thus showing the bone formation and remodeling in different parts of the callus.

Higher trabecular thickness and lower trabecular separation were generally considered

to represent a proper bone structure in cancellous bone development. However, lower trabecular thickness and higher trabecular separation might represent active callus remodeling during fracture healing, which in turn would accelerate fracture healing [71].

The osteoblast and osteoclast densities were defined as the ratios between cellular surface and mineralized bone surface [71, 95, 96]. Since higher bone surface is often linked with higher number of cells, the application of the cellular densities eliminates the bias possibly introduced by different callus sizes.

5 Conclusion

To conclude, the current study established the positive effect of TBI on the fracture healing in wild-type mice, while fracture healing in leptin-deficiency (ob/ob) mice was compromised. Furthermore, TBI could not reverse the impairing influence of leptin deficiency on fracture healing. Based on these findings, we suggest the involvement of leptin in the acceleration of fracture healing through the cascade signaling of TBI.

The pathophysiological process of fracture healing after TBI follows a complex mechanism. For clinical applications, comprehension of the biochemical and hormonal cascades of fracture healing after TBI could lead to the development of novel clinical therapies for delayed fracture healing and bone nonunion. Further investigation should concentrate on the cellular and molecular mechanisms of fracture healing after TBI in order to elucidate the feedback loops between bone and brain.

Bibliography

1. TA Einhorn, LC Gerstenfeld. Fracture healing: mechanisms and interventions. Nature reviews. Rheumatology, 11(1):45-54, 2015.
2. J Chalmers, DH Gray, J Rush. Observations on the induction of bone in soft tissues. Journal of bone and joint surgery (British), 57:36-45, 1975.
3. C Flin, H Curalucci, A Duvocelle, JM Viton. Heterotopic ossification and brain injury. Annual readaptive medicine in physics, 45:517-520, 2002.
4. DE Garland. Clinical observations on fractures and heterotopic ossification in the spinal cord and traumatic brain injured populations. Clinical and orthopedic related research, 233:86-101, 1988.
5. L Mendelson, Z Grosswasser, T Najenson, U Sandbank, P Solzi. Periarticular new bone formation in patients suffering from severe head injuries. Scandinavian journal of rehabilitation medicine, 7:141-145, 1975.
6. L Sazbon, T Najenson, M Tartakovsky, E Becker, Z Grosswasser. Widespread periarticular new-bone formation in long-term comatose patients. Journal of bone and joint surgery (British), 63-B:120-125, 1981.
7. PV Giannoudis, S Mushtaq, P Harwood, S Kambhampati, M Dimoutsos, Z Stavrou, HC Pape. Accelerated bone healing and excessive callus formation in patients with femoral fracture and head injury. Injury supplement, 37:18-24, 2006.
8. J Morley, S Marsh, E Drakoulakis. Does traumatic brain injury result in accelerated fracture healing. Injury, 36(3):363-368, 2005.
9. RF Spencer. The effect of head injury on fracture healing. A quantitative assessment. Journal of bone and joint surgery (British), 69:525-528, 1987.
10. DE Garland, B Rothi, RL Waters. Femoral fractures in head-injuries adults. Clinical orthopaedics and related research, no. 166, pp. 219-225, 1982.
11. OP Gautschi, D Cadosch, SP Frey, AP Skirving, L Filgueira, R Zellweger. Serum-mediated osteogenic effect in traumatic brain-injured patients. ANZ

Journal of surgery, vol. 79, no. 6, pp. 449–455, 2009.

12. D Cadosch, OP Gautschi, M Thyer. Humoral factors enhance fracture-healing and callus formation in patients with traumatic brain injury. The Journal of bone and joint surgery (American volume), vol. 91, no. 2, pp. 282-288, 2009.
13. TY Yang, TC Wang, YH Tsai, KC Huang. The effects of an injury to the brain on bone healing and callus formation in young adults with fractures of the femoral shaft. The Journal of bone and joint surgery (British volume), vol. 94, no. 2, pp. 227-230, 2012.
14. PV Giannoudis, S Mushtaq, P Harwood. Accelerated bone healing and excessive callus formation in patients with femoral fracture and head injury. Injury, vol. 37, supplement 3, pp. S18-S24, 2006.
15. J Andermahr, A Elsner, AE Brings, T Hensler, H Gerbershagen, A Jubel. Reduced collagen degradation in polytraumas with traumatic brain injury causes enhanced osteogenesis. Journal of Neurotrauma, vol. 23, no. 5, pp. 708-720, 2006.
16. R Perkins, AP Skirving. Callus formation and the rate of healing of femoral fractures in patients with head injuries. The Journal of bone and joint surgery (British volume), 69: 521-524, 1987.
17. W Huang, Z Li, Z Li, R Yang. Does traumatic brain injury result in accelerated mandibular fracture healing?. Journal of oral and maxillofacial surgery vol. 70, pp. 2135-42, 2012.
18. M. Boes, M. Kain, S. Kakar, F Nicholls, D Cullinane, L Gerstenfeld, TA Einhorn, P Tornetta. Osteogenic effects of traumatic brain injury on experimental fracture-healing. The Journal of bone and joint surgery (American volume), vol. 88, pp. 738-43, 2006.
19. Y Song, L Bi, Z Zhang, Z Huang, W Hou, X Lu, P Sun, Y Han. Increased levels of calcitonin gene-related peptide in serum accelerate fracture healing following traumatic brain injury. Molecular medicine reports, vol. 5, pp. 432-8, 2012.

20. L Wang, X Yao, L Xiao, XG Tang, H Ding, HX Zhang, JS Yuan. The effects of spinal cord injury on bone healing in patients with femoral fractures. The Journal of spinal cord medicine 37:4, pages 414-419, 2014.

21. DY Zhang, PX Zhang, YH Wang, N Han, C Tang, BG Jiang. The Influence of Brain Injury or Peripheral Nerve Injury on Calcitonin Gene-Related Peptide Concentration Variation and Fractures Healing Process. Artificial cells, blood substitutes, and biotechnology, 37:2, 85-91, 2009.

22. OP Gautschi, AM Toffoli, KA Joesbury, AP Skirving, L Filgueira, R Zellweger. Osteoinductive effects of cerebrospinal fluid from brain-injured patients. Journal of neurotrauma, 24:154-162, 2007.

23. P Ballabh, A Braun, M Nedergaard. The blood-brain barrier: an overview: structure, regulation, and clinical implications. Neurobiology of disease, 16:1-13, 2004.

24. SM Bidner, IM Rubins, JV Desjardins, DJ Zukor, D Goltzman. Evidence for a humoral mechanism for enhanced osteogenesis after head injury. Journal of bone and joint surgery (American volume), 72:1144-1149, 1990.

25. K Eid, L Labler, W Ertel, O Trentz, M Keel. Systemic effects of severe trauma on the function and apoptosis of human skeletal cells. Journal of bone and joint surgery (British volume), 88-B:1394-1400, 2006.

26. BY Klein, E Shohami, Y Reikhinshtein, H Ben-Bassat, M Liebergall. Serum-mediated osteogenic effects of head injury on cultured rat marrow stromal cells. Calcified tissue international, 65:217-222, 1999.

27. A Helmy, MG De Simoni, MR Guilfoyle, KL Carpenter, PJ Hutchinson. Cytokines and innate inflammation in the pathogenesis of human traumatic brain injury. Progress in neurobiology, 95:352-72, 2011

28. D. Cadosch, M. Thyer, OP Gautschi, G Lochnit, SP Frey, R. Zellweger, L. Filgueira, AP Skirving. Functional and proteomic analysis of serum and cerebrospinal fluid derived from patients with traumatic brain injury: a pilot study. ANZ journal of surgery, vol. 80, no. 7-8, pp. 542-7, 2010.

29. SG Yang, YH Ma, Y Liu, HP Que, CQ Zhu, SJ Liu. Arachidonic Acid: A

Bridge between Traumatic Brain Injury and Fracture Healing. Journal of neurotrauma, 20;29(17):2696-705, 2012.

30. Yan Y, Gong P, Jin W, Xu J, Wu X, Xu T, Hang Q, Fu H, Kei K, Gao Y. The cell-specific upregulation of bone morphogenetic protein-10 (BMP-10) in a model of rat cortical brain injury. Journal of molecule histology, 43:543-52, 2012
31. X. Liu, C. Zhou, Y. Li, Y. Ji, G. Xu, X. Wang, J. Yan. SDF-1 promotes endochondral bone repair during fracture healing at the traumatic brain injury condition. PloS one, vol. 8, p. e54077, Jan 2013.
32. Wildburger R, Zarkovic N, Leb G, Borovic S, Zarkovic K, Tatzber F. Post-traumatic changes in insulin-like growth factor type 1 and growth hormone in patients with bone fractures and traumatic brain injury. Wien Klinische Wochenschrift, 15;113(3-4):119-26, 2001.
33. YF Zhuang, Jie Li. Serum EGF and NGF levels of patients with brain injury and limb fracture. Asian pacific journal of tropical medicine, vol. 6, Issue 5, Pages 383-386, 2013,
34. H. Yan, HW Zhang, P Fu, BL Liu, WZ Jin, SB Duan, J Xue, K Liu, ZM Sun, XW Zeng. Leptin's effect on accelerated fracture healing after traumatic brain injury. Neurological research, vol. 35, pp. 537-44, 2013
35. Y Zhang, R Proenca, M Maffei, M Barone, L Leopold, JM Friedman. Positional cloning of the mouse obese gene and its human homologue. Nature, vol. 372, no. 6505, pp. 425-432, 1994.
36. M Wauters, RV Considine, LF Van Gaal. Human leptin: from an adipocyte hormone to an endocrine mediator. European journal of endocrinology, 143(3):293-311, 2000.
37. GR Hynes, PJ Jones. Leptin and its role in lipid metabolism. Current opinion lipidology, 12(3):321-7, 2001.
38. M Caprio, E Fabbrini, AM Isidori, A Aversa, A Fabbri. Leptin in reproduction. Trends endocrinology metabolism, 12(2):65-72, 2001.
39. Y Ogawa, H Masuzaki, K Nakao. Clinical implication of leptin, the obese

gene product. Internal medicine (Tokyo, Japan), 38(2):210-2, 1999.

40. G Frühbeck, SA Jebb, AM Prentice. Leptin: physiology and pathophysiology. Clinical physiology (Oxford England), 18(5):399-419, 1998.

41. JS Flier. Clinical review 94: What's in a name? In search of leptin's physiologic role. Journal of clinical endocrinology and metabolism, 83(5):1407-13, 1998.

42. PH van der Kroon, H Boldewijn, N Langeveld-Soeter. Congenital hypothyroidism in latent obese (ob/ob) mice. International Journal of obesity. 1982; 6(1):83–90.

43. AM Ingalls, MM Dickie, GD Snell. Obese, a new mutation in the house mouse. Obesity research, vol. 4, no. 1, p. 101, 1950.

44. AJ Kennedy, KL J Ellacott, VL King, AH Hasty. Mouse models of the metabolic syndrome. Disease models & mechanisms, vol. 3, no. 3-4, pp. 156–66, 2010.

45. SM Genuth, RJ Przybylski, DM Rosenberg. Insulin resistance in genetically obese, hyperglycemic mice. Endocrinology, vol. 88, no. 5, pp. 1230–1238, 1971.

46. P Ducy, M Amling, S Takeda, M Priemel, AF Schilling, FT Beil, J Shen, C Vinson, JM Rueger, G Karsenty. Leptin inhibits bone formation through a hypothalamic relay: a central control of bone mass. Cell, vol. 100, pp. 197–207, 2000.

47. S Takeda, F Elefteriou, R Levasseur, X Liu, L Zhao, KL Parker, D Armstrong, P Ducy, G Karsenty. Leptin regulates bone formation via the sympathetic nervous system. Cell. 2002 Nov 1;111(3):305-17.

48. MW Hamrick, C Pennington, D Newton, D Xie, C Isales. Leptin deficiency produces contrasting phenotypes in bones of the limb and spine. Bone, 34(3):376-83, 2004.

49. UT Iwaniec, S Boghossian, PD Lapke, RT Turner, SP Kalra. Central leptin gene therapy corrects skeletal abnormalities in leptin-deficient ob/ob mice.

Peptides, vol. 28, pp. 1012-9, 2007.

50. RT Turner, SP Kalra, CP Wong, KA Philbrick, LB Lindenmaier, S Boghossian, UT Iwaniec. Peripheral leptin regulates bone formation. Journal of bone and mineral research, vol. 28, pp. 22-34, 2013.
51. CM Steppan, DT Crawford, KL Chidsey-Frink, H Ke, AG Swick. Leptin is a potent stimulator of bone growth in ob/ob mice. Regulatory peptides, vol. 92, pp. 73–8, 2000.
52. R Yue, BO Zhou, IS Shimada, Z Zhao, SJ Morrison. Leptin Receptor Promotes Adipogenesis and Reduces Osteogenesis by Regulating Mesenchymal Stromal Cells in Adult Bone Marrow. Cell stem cell. 18(6):782-96, 2016.
53. JO Gordeladze, CA Drevon, U Syversen, JE Reseland. Leptin Stimulates Human Osteoblastic Cell Proliferation, De Novo Collagen Synthesis, and Mineralization: Impact on Differentiation Markers, Apoptosis, and Osteoclastic Signaling. Journal of cellular biochemistry, vol. 836, pp. 825-836, 2002.
54. T Thomas, F Gori, S Khosla, MD Jensen, B Burguera, BL Riggs. Leptin acts on human marrow stromal cells to enhance differentiation to osteoblasts and to inhibit differentiation to adipocytes. Endocrinology, vol. 140, no. 4, pp. 1630-1638, 1999.
55. L Wang, JS Yuan, HX Zhang, H Ding, Xg Tang YZ Wei. Effect of leptin on bone metabolism in rat model of traumatic brain injury and femoral fracture. Chinese journal of traumatology vol. 14, pp. 7-13, Feb. 2011.
56. Y Wei, L Wang, JC Clark, CR Dass PF Choong. Elevated leptin expression in a rat model of fracture and traumatic brain injury. The Journal of pharmacy and pharmacology, vol. 60, no. 12, pp. 1667-1672, 2008.
57. C Lin, SJ Huang, N Wang, ZP Shen. Relationship between plasma leptin levels and clinical outcomes of pediatric traumatic brain injury. Peptides, vol. 35, no. 2, pp. 166-171, 2012.
58. S Tsitsilonis, R Seemann, M Misch, F Wichlas, NP Haas, K Schmidt-Bleek,

C Kleber, KD Schaser. The effect of traumatic brain injury on bone healing: an experimental study in a novel in vivo animal model, Injury, vol. 46, no. 4, pp. 661-665, 2015.

59. KM Cheung, K Kaluarachi, G Andrew, W Lu, D Chan, KS Cheah. An externally fixed femoral fracture model for mice. Journal of orthopaedic research, vol. 21 pp. 685-90, 2003.

60. T Histing, JH Holstein, P Garcia, R Matthys, A Kristen, L Claes, MD Menger, T Pohlemann. Ex vivo analysis of rotational stiffness of different osteosynthesis techniques in mouse femur fracture. Journal of orthopaedic research, vol. 27 pp. 1152-6, 2009.

61. DH Smith, HD Soares, JS Pierce, KG Perlman, KE Saatman, DF Meaney, CE Dixon, TK McIntosh. A model of parasagittal controlled cortical impact in the mouse: cognitive and histopathologic effects. Journal of neurotrauma, vol. 12, pp. 169-78, 1995.

62. UW Thomale, M Griebenow, A Mautes, TF Beyer, NK Dohse, R Stroop, OW Sakowitz, AW Unterberg, JF Stover. Heterogeneous regional and temporal energetic impairment following controlled cortical impact injury in rats. Neurological research, vol. 29, no. 6, pp. 594-603, 2007.

63. UW Thomale, SN Kroppenstedt, TF Beyer, KD Schaser, AW Unterberg, JF Stover. Temporal profile of cortical perfusion and microcirculation after controlled cortical impact injury in rats. Journal of neurotrauma, vol. 19, pp. 403-13, 2002.

64. HZ Movat. Demonstration of all connective tissue elements in a single section; pentachrome stains. AMA archives of pathology. 60: 289–95, 1955.

65. AJ Olah, A Simon, M Gaudy, W Herrmann, RK Schenk. Differential staining of calcified tissues in plastic embedded microtome sections by a modification of Movat's pentachrome stain. Stain technology, 52(6):331-7, 1977.

66. FP van de Wijngaert, EH Burger. Demonstration of tartrate-resistant acid phosphatase in un-decalcified, glycolmethacrylate-embedded mouse bone: a

possible marker for (pre)osteoclast identification. Journal of histochemistry and cytochemistry, 34(10):1317-23, 1986.

67. M Mehta, P Strube, A Peters, C Perka, D Hutmacher, P Fratzl, GN Duda. Influences of age and mechanical stability on volume, microstructure, and mineralization of the fracture callus during bone healing: is osteoclast activity the key to age-related impaired healing?. Bone, vol. 47, pp. 219-28, 2010.

68. D Malhan, M Muelke, S Rosch, AB Schaefer, F Merboth, D Weisweiler, C Heiss, I Arganda-Carreras, TE Khassawna. An Optimized Approach to Perform Bone Histomorphometry. Frontiers in endocrinology (Lausanne), 21;9:666, doi: 10.3389/fendo. 2018.00666.

69. AM Parfitt, MK Drezner, FH Glorieux, JA Kanis, H Malluche, PJ Meunier, SM Ott, RR Recker. Bone histomorphometry: standardization of nomenclature, symbols, and units. Report of the ASBMR Histomorphometry Nomenclature Committee. Journal of bone and mineral research, 2(6):595-610, 1987.

70. DW Dempster, JE Compston, MK Drezner, FH Glorieux, JA Kanis, H Malluche, PJ Meunier, SM Ott, RR Recker, AM Parfitt.J Standardized nomenclature, symbols, and units for bone histomorphometry: a 2012 update of the report of the ASBMR Histomorphometry Nomenclature Committee. Journal of bone and mineral research, 28(1):2-17, 2013.

71. RJ van 't Hof, L Rose, E Bassonga, A Daroszewska. Open source software for semi-automated histomorphometry of bone resorption and formation parameters. Bone, 99:69-79, 2017.

72. M Maegele, P Riess, S Sauerland, B Bouillon, S Hess, TK McIntosh, A Mautes, M Brockmann, J Koebke, J Knifka, EA Neugebauer. Characterization of a new rat model of experimental combined neurotrauma. Shock, 23(5):476-81, 2005.

73. RJ Locher, T Lünnemann, A Garbe, KD Schaser, K Schmidt-Bleek, G Duda, S Tsitsilonis. Traumatic brain injury and bone healing:radiographic and

biomechanical analyses of bone formation and stability in a combined murine trauma model. Journal of musculoskeletal & neuronal Interactions, 15(4):309-315, 2015.

74. F Graef , R Seemann, A Garbe, K Schmidt-Bleek, KD Schaser, J Keller, G Duda, S Tsitsilonis. Impaired fracture healing with high non-union rates remains irreversible after traumatic brain injury in leptin-deficient mice. Journal of musculoskeletal & neuronal Interactions, 1;17(2):78-85, 2017.

75. FT Beil, F Barvencik, M Gebauer, B Beil, P Pogoda, JM Rueger, A Ignatius, T Schinke, M Amling. Effects of increased bone formation on fracture healing in mice. Journal of trauma, 70(4):857-62, 2011.

76. T Rőszer, T Józsa, ED Kiss-Tóth, N De Clerck, L Balogh. Leptin receptor deficient diabetic (db/db) mice are compromised in postnatal bone regeneration. Cell and tissue research, 356(1):195-206, 2014.

77. SN Khan, G DuRaine, SS Virk, J Fung, DJ Rowland, AH Reddi, MA Lee. The temporal role of leptin within fracture healing and the effect of local application of recombinant leptin on fracture healing. Journal of orthopaedic trauma, 27(11):656-62, 2013.

78. T Zhang, S Lin, X Shao, S Shi, Q Zhang, C Xue, Y Lin, B Zhu, X Cai. Regulating osteogenesis and adipogenesis in adipose-derived stem cells by controlling underlying substrate stiffness. Journal of cellular physiology, 233(4):3418-3428, 2018.

79. Q Chen, P Shou, L Zhang, C Xu, C Zheng, Y Han, W Li, Y Huang, X Zhang, C Shao, AI Roberts, AB Rabson, G Ren, Y Zhang, Y Wang, DT Denhardt, Y Shi. An osteopontin-integrin interaction plays a critical role in directing adipogenesis and osteogenesis by mesenchymal stem cells. Stem cells, 32(2):327-37, 2014.

80. H Kang, A Hata. The role of microRNAs in cell fate determination of mesenchymal stem cells: balancing adipogenesis and osteogenesis. BMB Report, 48(6):319-23, 2015.

81. ME Bateman, AL Strong, JA McLachlan, ME Burow, BA Bunnell. The

Effects of Endocrine Disruptors on Adipogenesis and Osteogenesis in Mesenchymal Stem Cells: A Review. Frontior Endocrinology (Lausanne), 9;7:171, 2017.

82. T Histing, P Garcia, JH Holstein, M Klein, R Matthys, R Nuetzi, R Steck, MW Laschke, T Wehner, R Bindl, S Recknagel, EK Stuermer, B Vollmar, B Wildemann, J Lienau, B Willie, A Peters, A Ignatius, T Pohlemann, L Claes, MD Menger. Small animal bone healing models: standards, tips, and pitfalls results of a consensus meeting. Bone, vol. 49, pp. 591-9, 2011.
83. O Jacenko, BR Olsen. Transgenic mouse models in studies of skeletal disorders. Journal of Rheumatology, vol. 22, pp. 39-41, 1995.
84. DM Nunamaker. Experimental models of fracture repair. Clinical orthopaedics and related research, pp. S56-S65, 1998.
85. L Claes, P Augat, G Suger, HJ Wilke. Influence of size and stability of the osteotomy gap on the success of fracture healing. Journal of orthopaedic research, vol. 15, pp. 577-84, 1997.
86. AE Goodship, J Kenwright. The influence of induced micromovement upon the healing of experimental tibial fractures. The Journal of bone and joint surgery (British volume), vol. 67, pp. 650-5, 1985.
87. J Kenwright, JB Richardson, AE Goodship, M Evans, DJ Kelly, AJ Spriggins, JH Newman, SJ Burrough, JD Harris, DI Rowley. Effect of controlled axial micromovement on healing of tibial fractures. Lancet, vol. 2, pp. 1185-7, 1986.
88. UW Thomale, K Schaser, SN Kroppenstedt, AW Unterberg, JF Stover. Cortical hypoperfusion precedes hyperperfusion following controlled cortical impact injury. Acta neurochirurgica. supplement, vol. 81, pp. 229-31, 2002.
89. CE Dixon, GL Clifton, JW Lighthall, AA Yaghmai, RL Hayes. A controlled cortical impact model of traumatic brain injury in the rat. Journal of neuroscience methods, vol. 39, pp. 253-62, 1991.
90. JW Lighthall. Controlled cortical impact: a new experimental brain injury model. Journal of neurotrauma, vol. 5, pp. 1-15, 1988.

91. DM Morales, N Marklund, D Lebold, HJ Thompson, A Pitkanen, WL Maxwell, L Longhi, H Laurer, M Maegele, E Neugebauer, DI Graham, N Stocchetti, TK McIntosh. Experimental models of traumatic brain injury: do we really need to build a better mousetrap?, Neuroscience, vol. 136, pp. 971-89, 2005.

92. E Martín-Badosa, D Amblard, S Nuzzo, A Elmoutaouakkil, L Vico, F. Peyrin. Excised bone structures in mice: imaging at three-dimensional synchrotron radiation micro CT. Radiology, vol. 229, no. 3, pp. 921-928, 2003.

93. ML Bouxsein, SK Boyd, B Christiansen, RE Guldberg, KJ Jepsen, R Müller. Guidelines for assessment of bone microstructure in rodents using microcomputed tomography. Journal of bone and mineral research, vol. 25, pp. 1468-86, 2010.

94. KM Reich, S Tangl, P Heimel, S Lettner, A Ignatius, LE Claes, J Pfeil, A Janousek, H Redl. Histomorphometric Analysis of Callus Formation Stimulated by Axial Dynamisation in a Standardised Ovine Osteotomy Model. Biomed research international, 2019:4250940, 2019.

95. MW Morcos, H Al-Jallad, J Li, C Farquharson, JL Millán, RC Hamdy, M Murshed. PHOSPHO1 is essential for normal bone fracture healing: An Animal Study. Bone joint research, 7(6):397-405, 2018.

96. RM Wong, U Thormann, MH Choy, YN Chim, MC Li, JY Wang, KS Leung, JC Cheng, V Alt, SK Chow, WH Cheung. A metaphyseal fracture rat model for mechanistic studies of osteoporotic bone healing. European cell & materials, 22;37:420-430, 2019.

Publications and conferences

Publications

R Seemann, F Graef, A Garbe, J Keller, **F Huang**, G Duda, K Schmidt-Bleek, KD Schaser, S Tsitsilonis. Leptin-deficiency eradicates the positive effect of traumatic brain injury on bone healing: histological analyses in a combined trauma mouse model. Journal of musculoskelet & neuronal Interaction, 1;18(1):32-41, 2018.

X Wang, J Huang, **F Huang**, JC Zong, X Tang, Y Liu, QF Zhang, Y Wang, L Chen, LJ Yin, BC He, ZL Deng. Bone morphogenetic protein 9 stimulates callus formation in osteoporotic rats during fracture healing. Molecular medicine reports, 15(5):2537-2545, 2017.

Conference

R Seemann, **F Huang**, A Garbe, F Graef, F Wichlas, K Schmidt-Bleek, KD Schaser, S Tsitsilonis. Histologische Merkmale der Knochenheilung im kombinierten Traumamodell bei Wildtyp- und Leptin-defizienter Maus. Deutscher Kongress für Orthopädie und Unfallchirurgie, 2015, Berlin, Deutschland

Curriculum Vitae/Lebenslauf

My curriculum vitae does not appear in the electronic version of my paper for reasons of data protection

My curriculum vitae does not appear in the electronic version of my paper for reasons of data protection

Affidavit

"I, Fan Huang, certify under penalty of perjury by my own signature that I have submitted the thesis on the topic 'Traumatic Brain Injury and Bone Healing: Histomorphometric Analyses of Bone Formation in a Wild-type and Leptin-deficiency Murine Model'. I wrote this thesis independently and without assistance from third parties, I used no other aids than the listed sources and resources.

All points based literally or in spirit on publications or presentations of other authors are, as such, in proper citations (see "uniform requirements for manuscripts (URM)" the ICMJE www.icmje.org) indicated. The sections on methodology (in particular practical work, laboratory requirements, statistical processing) and results (in particular images, graphics and tables) correspond to the URM (s.o) and are answered by me. My interest in any publications to this dissertation corresponds to those that are specified in the following joint declaration with the responsible person and supervisor. All publications resulting from this thesis and which I am author correspond to the URM (see above) and I am solely responsible.

The importance of this affidavit and the criminal consequences of a false affidavit (section 156,161 of the Criminal Code) are known to me and I understand the rights and responsibilities stated therein.

Date Signature

Acknowledgements

The writing of this medical dissertation has been a precious journey in my academic life. I could not have travelled this far without the passionate support of my supervisors, colleagues, and family during these years of study in Berlin.

First and foremost, I would like to express my heartfelt gratitude to my supervisor Prof. Dr. Klaus-Dieter Schaser and PD Dr. Serafeim Tsitsilonis, for the golden opportunity to perform my doctoral thesis in Charité - Universitätsmedizin Berlin. Their great research experience and patient guidance have a remarkable influence on my study.

Second, I am thankful to all members and colleagues from my research groups, who offer me their wonderful experiences and help. I am deeply indebted to PD Dr. Johannes Keller, Dr. Ricarda Seemann, Dr. Frank Graef and Anja Garbe, for their cordial help in the experimental designing, animal model and histomorphometric analyses. And I'm also grateful to Dr. Denise Jahn and Dr. Jessika Appelt, who helped me a lot in either experiments or my thesis revision. I highly appreciate the help and technical assistance from Gabriela Korus and Mario Thiele, the technicians of Julius Wolff Institute in my study. Furthermore, I am grateful for financial support from the China Scholarship Council.

Finally, special thanks go to my parents for their unconditional support. And thank you Li for the great adventure that we share. Without their endless love and support, I can never achieve all these.